POLITECNICO
MILANO 1863

SCUOLA DI INGEGNERIA INDUSTRIALE
E DELL'INFORMAZIONE

Predictive Control and Estimation in a real District Heating Network

Tesi di Laurea Magistrale in
Automation and Control Engineering - Ingegneria dell'Automazione

Author: **Marco Tognacca**

Student ID: 10669099
Advisor: Prof. Alessio La Bella
Co-advisors: Ing. Lorenzo Nigro, Ing. Claudio Anderis
Academic Year: 2023-24

Alla mia nonna

Abstract

A district heating system is an energy plant aimed at distributing heat through thermally insulated water pipelines, used for both residential and commercial purposes. It consists of a generation section, which can utilize various energy sources for heat production, a distribution section, and a consumption section (the users).
The purpose of this thesis is to design a Model Predictive Control (MPC) scheme for a test district heating plant located at RSE SpA (Via Raffaele Rubattino, 54, 20134 Milan). The plant includes a generation station composed of a gas boiler, an electric boiler, and a combined heat and power unit (CHP), while the users are simulated by four heat exchangers that dissipate the received heat through a cooling circuit.
The Model Predictive Control (MPC) algorithm is developed to optimize the system's performance in terms of power usage and efficiency. The nonlinear model formulation (NMPC) is illustrated, including the constraints on states and inputs, as well as the corresponding cost function. Additionally, a Moving Horizon Estimation algorithm is presented, which estimates all unmeasurable states of the network based on available sensor measurements. Finally, the implementation of the control scheme on the actual plant is described, and the results obtained from the experimental campaign are discussed.

Keywords: District Heating Networks, Model Predictive Control, Moving Horizon Estimator

Abstract in lingua italiana

Un sistema di teleriscaldamento è un impianto energetico finalizzato alla distribuzione di calore per mezzo di condotte d'acqua isolate termicamente, utilizzato sia a fini residenziali sia commerciali. È costituito da una parte di generazione, che può sfruttare diverse fonti energetiche per la produzione di calore, da una parte di distribuzione e da quella di consumo (le utenze).
Lo scopo di questa tesi è quello di realizzare uno schema di controllo di tipo Model Predictive Control per un impianto di teleriscaldamento di prova, situato presso RSE SpA (Via Raffaele Rubattino, 54, 20134 Milano). L'impianto comprende una parte generativa formata da un boiler a gas, un boiler elettrico e un co-generatore (CHP), mentre le utenze vengono simulate da quattro scambiatori di calore che permettono di dissipare il calore ricevuto grazie a un circuito di raffreddamento.
L'algoritmo di Model Predictive Control (MPC) viene sviluppato al fine di ottimizzare il comportamento del sistema, in termini di potenza utilizzata ed efficienza. Viene illustrata la formulazione non lineare del modello (NMPC), presentandone i vincoli sugli stati e sugli ingressi e la relativa funzione di costo. Viene inoltre presentato un algoritmo di Moving Horizon Estimation che permette di stimare tutti gli stati non misurabili della rete, basandosi sulle misurazioni dei sensori che sono disponibili. Infine viene descritta l'implementazione dello schema di controllo sull'impianto reale e vengono discussi i risultati ottenuti dalla campagna sperimentale.

Parole chiave: Sistemi di teleriscaldamento, Model Predictive Control, Moving Horizon Estimator

Contents

Introduction

Motivation

As anyone knows, the problem of the global warming is of particular interest nowadays since it causes the raise in the Earth's average temperature. The global average temperature has in fact increased by 1.1 degrees Celsius with respect to the pre-industrial period and, to prevent warming beyond 1.5°C, we need to reduce emissions by 7.6 % every year from now until 2030 [28].

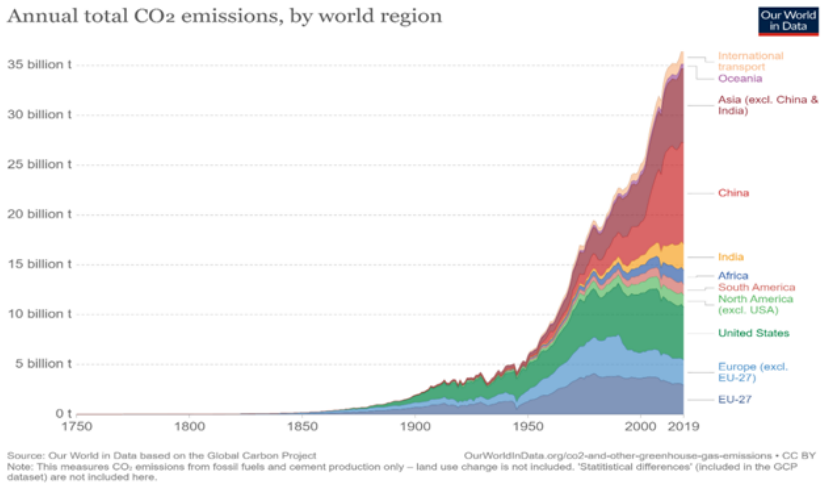

Figure 1: Annual CO_2 emissions (image taken from [9]).

Among the objectives set by the European Union to prevent from the global warming, there are the reduction of greenhouse gas emissions, the increase in the share of renewable energy, and the improvement of energy efficiency. For example, Italy, to achieve this goal, has committed to increase its photovoltaic and wind power production capacity by approximately 32 GW and 10 GW, respectively. Therefore, by 2030, an installed capacity of 52 GW for photovoltaic and 19.3 GW for wind power is expected [30]. This requires a transformation process of the entire energy system, with greater emphasis on the use of energy from renewable sources. For this reason, the study of multi-energy systems

becomes of primary importance [26]: these are systems in which different energy vectors, such as electricity, gas, and heat, optimally cooperate together, as one can see in Figure 3.1.

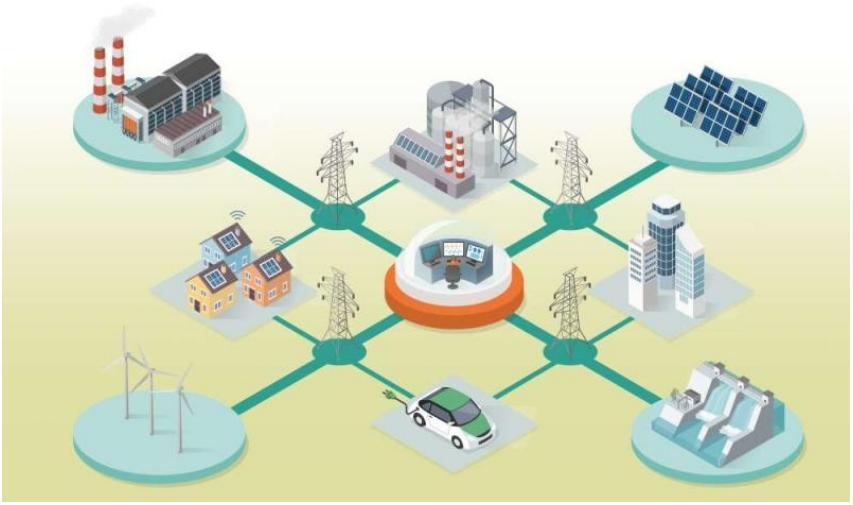

Figure 2: Multi energy system, different energy vectors cooperating together (image taken from [6].

The sustainability of multi-energy systems derives both from the possibility of making greater use of non-predictable renewable sources and from the increased efficiency and flexibility achieved. To make an example, multi energy systems are able to manage the problem of "over-generation" caused by some types of renewable sources such as the solar one. In fact photovoltaic electricity production is concentrated precisely in the central hours of the day, and, although historically the peak daily demand is recorded during this time, it is expected that production may still exceed the demand for electricity. Consequently, in such cases, it becomes normally necessary to disconnect renewable production to avoid problems on the grid. The application of a multi-energy system, on the other hand, would allow the conversion of surplus electricity into another energy vector, such as the thermal energy (*"power-to-heat"*) [30]. In this way, the energy could be stored or even used locally in a different form.
Multi-energy systems, however, are not potentially limited only to the synergy between electrical and thermal vectors; they can also offer integration possibilities with other energy vectors and exploit their infrastructures. One of the infrastructures that could potentially benefit from a multi-energy application is the gas network, especially in Italy where it extends across almost the entire national territory. In this regard, a study conducted in Great Britain analyzed the possibility of converting renewable electrical energy

into hydrogen on a national scale to inject it into the gas transmission network (*"power-to-gas"*). The study stemmed from the need to avoid the disconnections of wind power production from the electrical grid in light of the installation of new plants mainly in the north of Great Britain. Forced disconnections were expected on very windy days due to low electricity demand during the early hours of the day, to the highly congested transmission line from north to south of Great Britain, and to the limited flexibility offered by the nuclear power plants in the British energy system. The study shows that the use of electrolysers to produce hydrogen and inject it into the gas infrastructure, could significantly reduce wind farm disconnections during periods of strong wind. However, injecting even small percentages of hydrogen into the gas network can cause problems for consumers, which is why such injections are still under experimentation [30].

In conclusion, it's clear that a good optimization of this type of systems is fundamental to reach the goals of having a better energy efficiency and reducing emissions. Usual control strategies, such as PID control, are unable to meet these objectives, and as a consequence the implementation of "advanced control techniques" is needed [1]. Therefore, Model Predictive Control is the best choice, since it can compute a prediction about the future behavior of the system and, by minimizing a suitable cost function, is able to find the control action to be applied to the system itself. The advantage of this control method is exactly the fact that the applied control action is the best one possible, being obtained as a result of an optimization problem based on constraints on inputs, outputs or states.

Literature review

Concerning the simulation of DHN, a precise model is pivotal to accurately simulate thermo-hydraulic dynamical behavior [25]. Simulators can be based on detailed modeling libraries for thermohydraulic systems, for example, the *ThermoPower* library developed in Modelica [5]. Nevertheless, these simulation environments require numerous physical parameters that may be unavailable. Moreover, they model dynamics that are less relevant for DHNs (e.g., fluid phase transition) leading to additional computational effort and slower simulations, often without useful information return. Consequently, optimization-based regulators through the mentioned environments may be not practical.
Concerning the design of MPC controllers for DHN systems, some works have been proposed in the literature, but these brought to issues in terms of computational efficiency, [22], or large scale non-linearities, [13]. Hence, most of the existing solutions to decrease the computational complexity of MPC regulators for DHN systems rely on simplified

models. These simplifications could regard the negligibility of temperature dynamics over network pipelines, [27] and [7], or fixed transport delays and water flow, [23]. Other possibilities have also been explored, but none of these solutions enable to properly consider heating network inertia and constraints.
This discussion motivates the necessity of developing novel control-oriented DHN models, computationally efficient and accurate enough to properly represent the network thermal dynamics [19]. Existing works on detailed DHN models neglect fundamental elements or involve demanding simulations being not focused on DHN systems, e.g. [4]. This means that existing control strategies for this type of systems rely on highly complex models unsuitable for optimal predictive control, e.g. [12]. Hence, the present work aims to extend and deepen the results in [17], which explored District Heating Systems (DHSs) in detail from a control-oriented perspective, including the development of a Modelica library called *DHN4Control*. In this manuscript, the main objective is to study DHSs and the involved dynamics for their modeling and optimal control. As explained also in [19], a methodology for deriving a control-oriented DHN model was obtained, suitable for designing a nonlinear model predictive control (NMPC) regulator, ensuring computationally efficient and cost-effective regulation while respecting operative constraints [19]. The aim of this thesis is to expand upon these studies, leveraging the opportunity to implement the control scheme on a real plant: the Test Facility at Ricerca sul Sistema Energetico - RSE SpA [2].

Main contribution and case study

As introduced in the above section, this thesis aims at capturing relevant dynamics of DHNs while discarding negligible ones, for example pressure differences across the network as will be explained in Chapter 2. Furthermore, as already said, the designed control strategy will be applied on the real Test Facility plant in order to observe how an MPC regulator (designed using a reduced control-oriented model) behaves when connected to a physical system, instead of doing it only through simulation.
The case of study is the facility located at Ricerca sul Sistema Energetico - RSE S.p.A. (Via Raffaele Rubattino, 54, 20134 Milano). RSE has realized a multi energy system including electrical and thermal energy vectors, integrating a new district heating network into the existing electric micro-grid of the "Distributed Energy Resources Test Facility" Laboratory. The plant has been realized based on a benchmark (A2A Milano - Canavese Thermal Power Plant, 2017 data) and using the existing co-generator installed in the RSE Test Facility, by scaling all the other components. The plant is characterized by

different components such as two boilers (one electric and one gas powered), chiller, co-generator, storage tanks, and heat exchangers, and its control system is based on PLCs. Furthermore, the plant was built in such a way as to allow for the modification of the configuration to enable operation in both traditional district heating system setup (with *centralized heat generation*) and innovative setup (with *distributed generation*). As a final remark, the facility has the possibility of integrating, in future, new components and different energy systems (e.g., *power-to-gas*) [30]. The Test Facility plant will be analyzed in details in Chapter 1.

Figure 3: A view of the RSE Test Facility (image taken from [24]).

Thesis outline

The structure of the thesis is the following:

- **Chapter 1**: Initially, a description of the RSE Test Facility is presented; then the plant is analyzed component by component providing and explaining the characteristic equations governing it. Finally a brief discussion on the control schemes currently implemented in the Test Facility is presented, highlighting their roles in optimizing plant performance and stability.
- **Chapter 2**: Starting from the equations outlined in Chapter 1, the MPC reduced model is described, with an analysis of each part of the plant and corresponding model validation. The validation is performed using both the Modelica simulator (RSE library *MultiEnergySystem*) and real data obtained directly from tests conducted on the Test Facility.
- **Chapter 3**: The problem of the initialization for the MPC, and consequently the development of the observer, is addressed: Moving Horizon Estimator is presented, including details on the sensors it utilizes. Then, a validation using simulator and real data is performed. Lastly, some strengths of the estimator are highlighted.
- **Chapter 4**: The MPC control scheme (including MHE) is connected to the real system through a Python script and tested online. The obtained and control performances are discussed.
- **Conclusions**: A brief recap of the thesis is given by commenting the obtained results of MPC and MHE. Finally a little discussion about possible future developments.

1 | System modeling

To achieve the goal of the thesis, first of all, it is necessary to present the whole dynamic model of the considered case study and the software used for the simulation. The following chapter will present the real plant of the RSE Test Facility, component by component, and the software choice used to model it. Along with each element of the network, its correspondent non linear equations are written and explained.

1.1. Test Facility plant

In this section, the real plant of the Test Facility situated in RSE SpA is presented in details and the mathematical equations modelling its dynamics are formulated.

1.1.1. Plant description

As already said in the Introduction, the RSE Multi Energy System consists of a district heating network (DHN) integrated with the existing low-voltage experimental micro-grid, known as the Distributed Generation Test Facility. The district heating network has been designed with a block logic, where each block represents a "plant system"; it is possible to operate the network with all systems running or with only some of them [31]. The district heating network is constructed with a *rack* structure, so that every subsystems was constructed in the workshop while, at the RSE site, the interconnections between the main components (as well as the electrical connections and insulation) was carried out. The network is also equipped with an auxiliary cooling circuit necessary for simulating the dissipation of heat by the users.
As can be seen in Figure 1.1, heated water (red arrows) flows from the generators to the centralized rack where it mixes, then reaches the four heat exchangers passing through the "primary pump" (in green on the left) and the rack distribution. Once arriving at the loads, heated water is cooled by interacting with cold water of the cooling circuit (light green arrows connecting chiller and loads). Finally cooled water goes back to the

generators where it will be reheated (blue arrows), while warmed water in the other circuit goes back to the chiller, thanks to the "secondary pump", where it will be cooled again (light blue arrows).

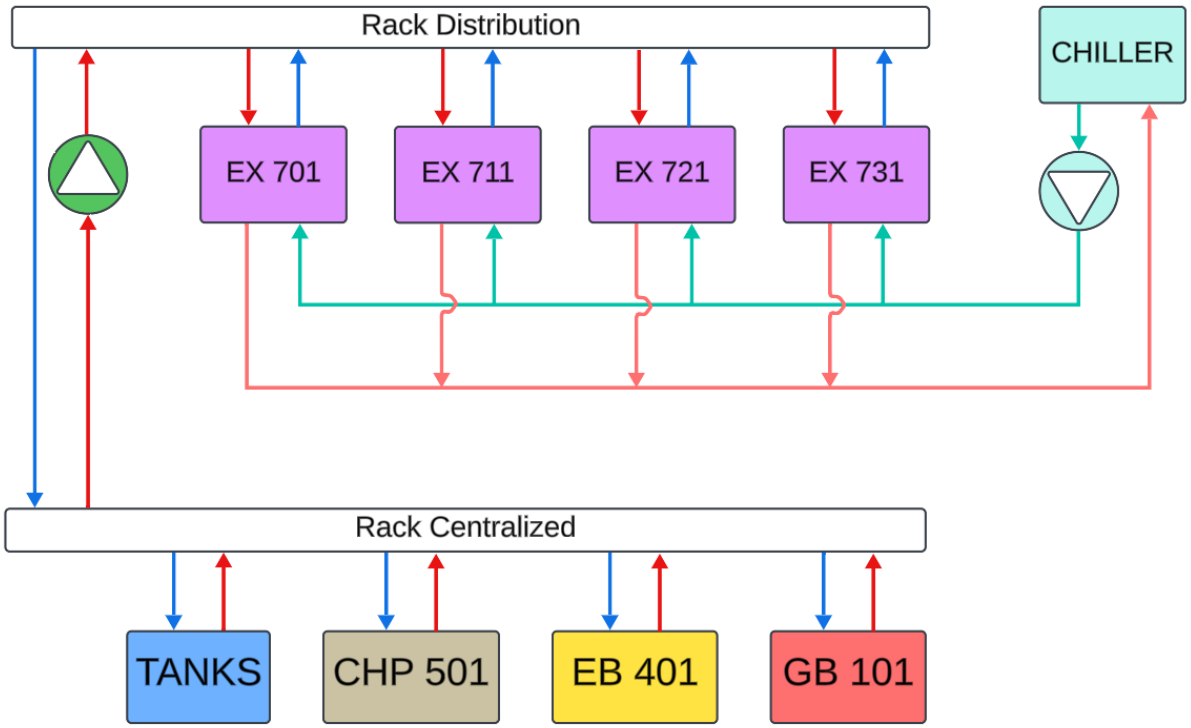

Figure 1.1: Structure of the District Heating Network case study. A more detailed scheme is in Section 1.3

.

The district heating network has a nominal capacity of approximately 200 kW_{th}, corresponding to the maximum thermal power of the loads (four heat exchangers of 50 kW_{th} each). Heat generation can be managed by appropriately modulating the different generators based on the operational conditions required by the plant; the total thermal power of the generators is about 365 kW_{th}. The pipes of the Facility are built for heating systems with temperatures ranging between -20 °C and +120 °C and pressure up to a maximum of 16 bar; however, the maximum temperature and pressure of the plant are 95 °C and 5.5 bar, respectively. In normal operating conditions, plant pressure stays in the range of 2-4 bar, while temperature is around 80 °C for the supply lines and 60 °C for the return lines. The plant can also operate at lower temperatures to emulate new generation district heating networks. Plant fluid is demineralized water [24]. A brief summary of the key information is written in Table 1.1. A simulator of the whole plant has been developed directly by RSE SpA in Modelica language, as stated in Section 1.2, to analyze the system dynamics in a simulation framework. Figure 1.2 shows a picture of the real RSE Test

Facility, in particular the rack centralized on the left and the rack distribution on the right (image taken from [24]).

Figure 1.2: Photo of the real RSE Test Facility plant.

1.1.2. Heat generation section

Gas Boiler "GB"

Gas boilers are heating systems that use gas to heat water, providing hot water for residential and commercial buildings. They operate by burning gas in a combustion chamber and transferring heat to the water circulating through a series of pipes; this heated water can finally be distributed to warm up buildings.
The Gas Boiler of the Test Facility has a maximum power of 147 kW_{th}. This power allows for meeting the base load of the users (around 125 kW_{th}). The boiler is controllable by imposing a temperature setpoint on the output using an internal controller, i.e. it can sets the desired supply temperature. Its connection with the rest of the plant is realized with a flow mass pump (so that it regulates the water mass flow), and a valve. Figure 1.4 shows a picture of the real gas boiler implemented in the Test Facility (image taken from [24]).
The Gas Boiler operates in steady state conditions in terms of mass flow rate $\dot{m}$, whereas the pressure p undergoes a decrease according to Stevin's law, as expressed in Equations (1.1) and (1.2).

$$\dot{m}_{in} = \dot{m}_{out} \tag{1.1}$$

$$p_{in} - p_{out} = \rho \cdot g \cdot h \tag{1.2}$$

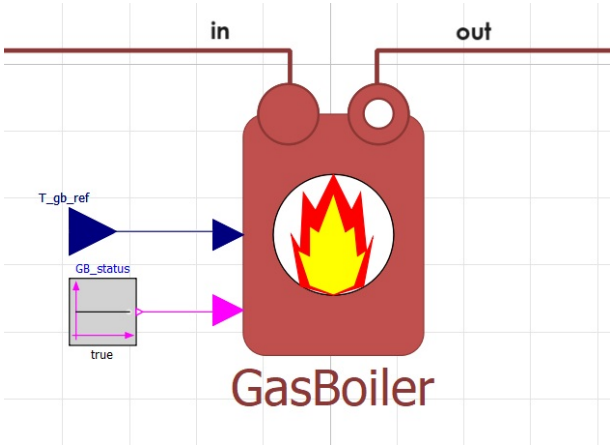

Figure 1.3: Gas Boiler block in the RSE *MultiEnergySystem* library.

where ρ is the water density, g the gravitational acceleration constant and h the height of the boiler. The characteristic equation of the boiler defining the behavior of the outlet temperature is reported in Equation (1.3) and depends on both the inlet and outlet enthalpy of the fluid and on the power exchanged with water (P_{heat}) and that one lost towards the ambient (Q_{amb}).

$$Mc_p\dot{T}_{out} = \dot{m}_{out}h_{out} + \dot{m}_{in}h_{in} + P_{heat} - Q_{amb} \tag{1.3}$$

where $M = \rho V = \rho h\frac{D^2}{4}$ represents the nominal mass of the fluid container, i.e. the boiler, while c_p is the specific heat for water at 80 °C. The last two terms are computed recalling that P_{heat} depends on the mass flow rate of the fuel, while Q_{amb} depends on the temperature difference with the external environment. The latter in particular follows the expression in Equation (1.4) and is based on two quantities: R_{lat}, the thermal resistance [K/W] computed approximating the TES with a cylinder, and R_{flat}, the flat Surface of the cylinder.

$$Q_{amb} = \frac{1}{R_{lat} + 2R_{flat}}(T_{out} - T_{ext}) \tag{1.4}$$

Figure 1.4: Photo of the gas boiler implemented in the RSE Test Facility.

Electric Boiler "EB"

Electric boilers are heating devices similar to gas boilers, but, to heat water for domestic and industrial purposes, they don't use fuel but electricity. They can offer high efficiency and precise temperature control and, unlike gas boilers, they produce no emissions, making them environmentally friendly.

The Electric Boiler implemented in the Test Facility, shown in Figure 1.6 (image taken from [24]), has a maximum power P_{heat} of 50 $\mathrm{kW_{th}}$ given by the product of the total number of resistors, five, and of the electric power of each one of them, 10 $\mathrm{kW_{th}}$. As the gas boiler, it can be temperature controlled by setting the reference for the water in the supply line and it is also equipped with a flow mass pump and a valve to regulate the flow rate passing through. The equations describing the electric boiler are similar to those ones for the gas boiler, except for the computation of P_{heat}, which has been already explained, and it is related to the outlet boiler temperature through Equation (1.5).

$$P_{heat} = \dot{m}_{in} \cdot c_p \cdot (T_{out,ref} - T_{in}) \tag{1.5}$$

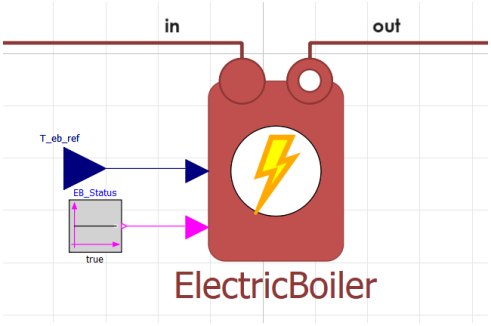

Figure 1.5: Modelica block of the Electric Boiler.

Figure 1.6: Photo of the electric boiler used in the RSE Test Facility.

Combined Heat and Power "CHP"

Combined Heat and Power (CHP), also known as co-generator, is an efficient energy system that at the same time generates electricity and useful thermal energy from a single fuel source. Its operating principle is conceptually easy: the CHP produces electrical power by burning fuel, which could be natural gas, biomass or waste products, and simultaneously captures the produced heat (that in traditional power generation would otherwise be wasted) through a heat exchanger to warm water. In this way this type of systems achieves greater energy efficiency, often exceeding 80% [10], that makes them widely used in industrial, commercial, and residential applications, offering significant cost savings and environmental benefits.

The CHP placed in the Test Facility is the one on which the scaling of values for simulating a real network was based, as presented in the introduction. Figure 1.8 (from document [24]) shows a picture of the real CHP and in particular of its heat exchanger network. This

generator can guarantee 50 kW_{th} of electrical power and 81 kW_{th} of thermal one. One can settle the reference electrical power $P_{electrical,ref}$ to be produced and the thermal power $P_{heat,ref}$ that is transferred to the water through the heat exchanger can be computed as a fraction of it, following the relation in Equation (2.7). Considering $\eta_{thermal} = 0.5453$ and $\eta_{electrical} = 0.4193$, respectively, the efficiencies referred to the thermal and electrical power production the CHP follows Equation (2.7). Once thermal power is computed, the correlation between mass flow, outlet temperature and power can be found as in Equation (1.7).

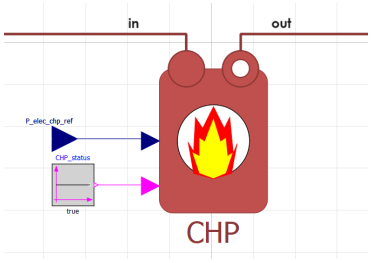

Figure 1.7: Modelica block of the CHP.

$$P_{heat,ref} = \frac{P_{electrical,ref}}{\eta_{electrical}} \cdot \eta_{thermal} \tag{1.6}$$

$$P_{heat,ref} = \dot{m}_{in} \cdot c_p \cdot (T_{out,ref} - T_{in}) \tag{1.7}$$

Figure 1.8: CHP system of the RSE Test Facility.

1.1.3. Thermal Storage "ST"

Thermal storage is useful to ensure more stable operating conditions and to allow better integration between different systems (in this case, electrical and thermal): it stores excess energy during periods of low demand and release it when demand is high, improving grid stability and reliability [6]. The TES is connected to the supply and return distribution networks and can absorb/inject water from/to each network through a local pump, as can be seen in Figure 1.9 or in Figure 1.24 for further details. In the RSE Test Facility it consists of two insulated cylindrical tanks, 5 m tall and with an external diameter of 1.9 m, for a total volume of approximately 10 m^3 each. Figure 1.11 displays a photo of the real TES implemented in the Test Facility network (image taken from [24]).

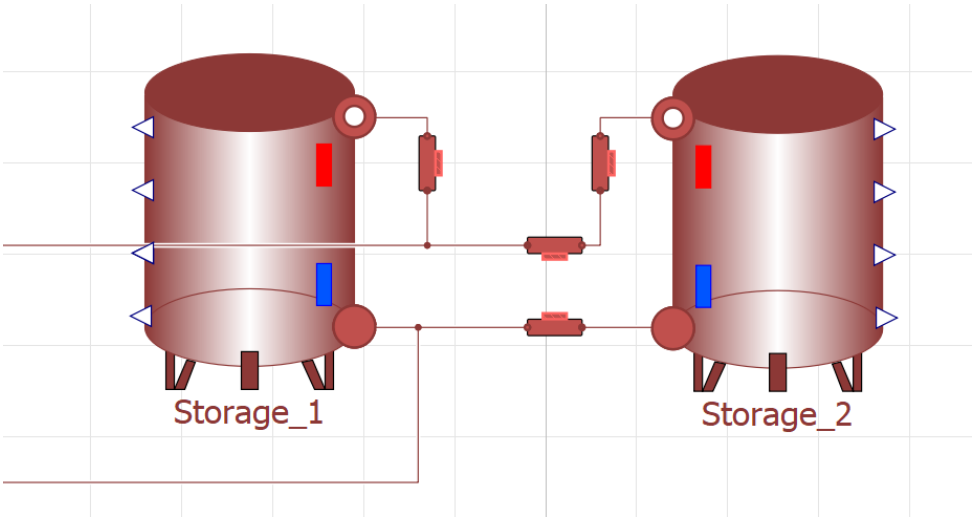

Figure 1.9: Modelica model of the two Test Facility tanks connected together.

Recently, complex models based on fluid dynamics have been developed to describe TES in three dimensions and represents its thermal behavior spatially. However, it has been shown that one-dimensional models are sufficient to characterize with enough accuracy temperature variations along the height of the tank [3]. For this reason, a stratified model has been adopted [18], as illustrated in Figure 1.10: each one of the two tanks is divided into n sections, in this case four sections, whose boundaries are orthogonal to the water flow direction. Being the tanks cylindrical, every section k has an height $h_k = h = \frac{H}{n} = 1.25\ m$ and a volume $v_k = v = h_k \pi r^2 = 2.5\ m^3$ (the radius r is constant being not dependent on the considered section). The thermal storage water flow, $q(t)$, is bidirectional and, as a convention, it has been chosen that $q(t) > 0$ when flowing from the return to the supply network ("mass flow discharge") and $q(t) < 0$ when flowing in the opposite direction ("mass flow charge"). However, it's not possible to have both charge and discharge simultaneously: a constraint for TES is in fact that the product between

these two mass flows is always equal to zero, as will be explained in Section 2.4.6.
As already said, a very detailed model is not necessary to describe the thermal behavior of TES: internal velocities and forces over the temperatures of the tank layers are negligible [3]; thus, the momentum conservation law is not required. Also mass balance is useless since the tank is always maintained full of water. Hence the only needed balance equation is the energy conservation law. Thus, considering the TES divided in four sections, for each $k \in \{1, ..., 4\}$ of a certain tank, the temperature model is defined as in Equation (1.8) [18]:

$$\begin{aligned} c_p \rho_k v \dot{T}_k(t) = \; & 2\pi r h \alpha (T^e(t) - T_k(t)) + \\ & + \pi r^2 \kappa ((T_{k+1}(t) - T_k(t)) + (T_{k-1}(t) - T_k(t))) + \\ & + c_p q(t) \begin{cases} T_{k-1}(t) - T_k(t) & if \quad q(t) \geq 0 \\ T_k(t) - T_{k+1}(t) & if \quad q(t) < 0 \end{cases} \end{aligned} \tag{1.8}$$

where r and h are respectively the radius of the TES and the height of a layer ($h = \frac{H}{4}$), see Figure 1.10, α is the coefficient related to losses towards the environment, $T^e(t)$ represents the external temperature and $T_0(t)$ (i.e. T_{k-1} when $k = 1$) and $T_5(t)$ (i.e. T_{k+1} when $k = 4$) stand for the supply and return temperatures, respectively. κ is instead a coefficient regarding the thermal exchange between different layers.
Another simplifying assumption is that the heat flux between tank walls and ambient can be neglected given that thermal storages in DH systems are typically well insulated. Finally, applying Equation (1.8) to each layer and neglecting the heat dissipation towards external environment, a TES thermal dynamic model is defined as in Equation (1.9) [3].

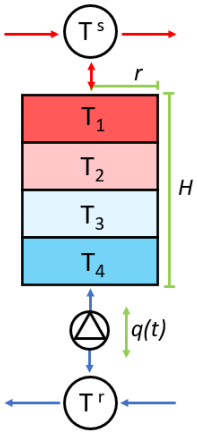

Figure 1.10: Model of the stratified Thermal Storage tank. T^s and T^r stand for supply and return temperature.

$$
\begin{aligned}
&\textbf{Layer} \quad \textbf{1:} \\
&\rho c_p A h \dot{T}_1 = c_p \dot{m}_{charge}(T_{charge} - T_1) + c_p \dot{m}_{discharge}(T_2 - T_1) + \frac{kA}{h}(T_2 - T_1) \\
&\textbf{Layer} \quad \boldsymbol{i} = \textbf{2,...,}\boldsymbol{n}\textbf{-1:} \\
&\rho c_p A h \dot{T}_i = c_p \dot{m}_{charge}(T_{i-1} - T_i) + c_p \dot{m}_{discharge}(T_{i+1} - T_i) + \frac{kA}{h}(T_{i+1} - 2T_i + T_{i-1}) \\
&\textbf{Layer} \quad \boldsymbol{n}\textbf{:} \\
&\rho c_p A h \dot{T}_n = c_p \dot{m}_{discharge}(T_{discharge} - T_n) + c_p \dot{m}_{charge}(T_{n-1} - T_n) + \frac{kA}{h}(T_{n-1} - T_n)
\end{aligned}
\tag{1.9}
$$

where $\dot{m}_{charge}$ represents the water mass flow $q(t)$ when the latter is negative, while $\dot{m}_{discharge}$ when it's positive. T_{charge} and $T_{discharge}$ correspond respectively to T^s and T^r of Figure 1.10. Lastly, the therm $\frac{kA}{h}$ is a coefficient related to the thermal exchange between different sections. It must be kept into consideration one of the main constraints related to thermal storage, explained in Section 2.4.6, which is the possibility of having m_{charge} or $m_{discharge}$ only one at a time. Thus the product between these two variables must be null.

Figure 1.11: Photo of the Test Facility thermal storages.

1.1.4. Primary pump

The primary pump is positioned in the primary network (that one represented by red and blue arrows in Figure 1.1) to guarantee a given pressure drop at its ports regardless the mass flow rate of water passing through it. This component is fundamental since a variable mass flow rate causes pressure variations in the plant which can compromise other components workflow, in particular of those ones that operate in steady state such as boiler and CHP.

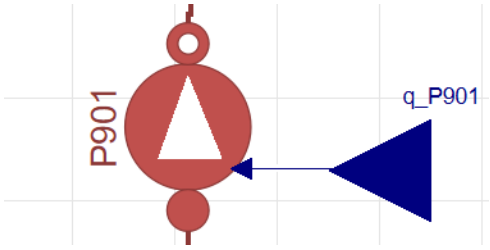

Figure 1.12: Modelica block for the primary pump.

The water pump has no storage of mass or energy and it's modeled through the head characteristic equation, Equation (1.10):

$$H = \left(\frac{\omega}{\omega_{nom}}\right)^2 \cdot \left(a_1 + a_2 q \frac{\omega_{nom}}{\omega} + a_3 \left(q \frac{\omega_{nom}}{\omega}\right)^2\right) \tag{1.10}$$

where a_i are the coefficients describing the characteristic curve of the pump, H is the pump head, ω and ω_{nom} the angular velocity and the nominal angular velocity, q the volumetric flow rate. Pump head H is a function of the pressure drop Δp between the inlet and the outlet of the pump. In conclusion, the equations governing the pump dynamics and thus modeling this component are here reported:

$$\begin{cases} p_{out} - p_{in} = \Delta p \\ T_{in} = T_{out} \\ m_{in} + m_{out} = 0 \end{cases} \tag{1.11}$$

1.1.5. Cooling System

Thermal Loads "EX"

The thermal load represents the heat consumption due to the users, i.e. it replicates the residential, commercial or industrial buildings to be heated. The value derived from scaling was approximately 125 kW_{th}, but it was decided to increase this amount of power to a total of around 200 kW_{th} to broaden the system's range of use. The thermal load is implemented through four independent heat exchangers of 50 kW_{th} each. In this way, in addition to having a total load of 200 kW_{th}, it is possible, under conditions of lower thermal load such as the scaling value, to distribute the loads differently among the various users, creating conditions of non-uniformity in the district heating circuit. Figure 1.15 (taken from [24]) shows a picture of one of the heat exchangers connected to the real network.
Heat exchangers and their relative equations are analyzed in the following subsection, while subsection "Power control" presents the control scheme which regulates heat exchangers in the RSE Test Facility.

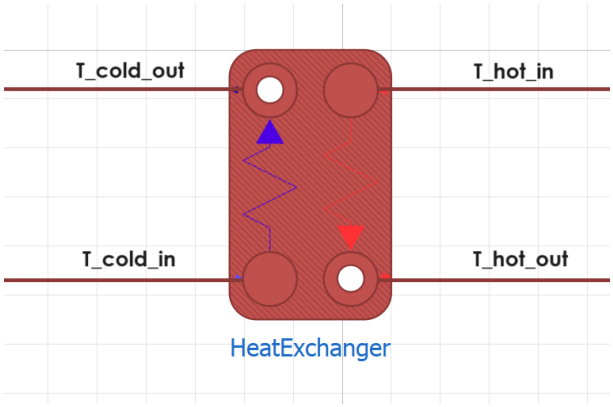

Figure 1.13: Modelica block of a single heat exchanger. The cold side (blue arrows) is referred to the cooling circuit, while the hot side is the network connected with the generation section

Heat exchangers - Thermodynamic analysis

A heat exchanger is defined as a physical device which allows the passage of thermal energy from a fluid with greater temperature to a fluid with lower temperature. There are several types of heat exchangers, based on the shape and on the direction of the two flowing fluids. Before going into details with the analysis, some assumptions have to be

considered [29]:

- it will be considered a system with only one inlet and outlet for each fluid (hot and cold);
- kinetic and potential terms of energy will be neglected;
- thermal power losses towards the ambient will be neglected, too.

In figure Figure 1.14 there is the reference model of a heat exchanger; for simplicity it's reported the model of a heat exchanger with *coaxial tubes*, where the hot fluid flows in a pipe around which the cold fluid flows, but the analysis could be extended also for other structures. This scheme is in "counter-current" configuration. In this reference model four arrows are reported, representing the inlet and outlet of the hot fluid and the inlet and outlet of the cold fluid. First, the balances that describe the behavior of the heat exchanger have to be analyzed.

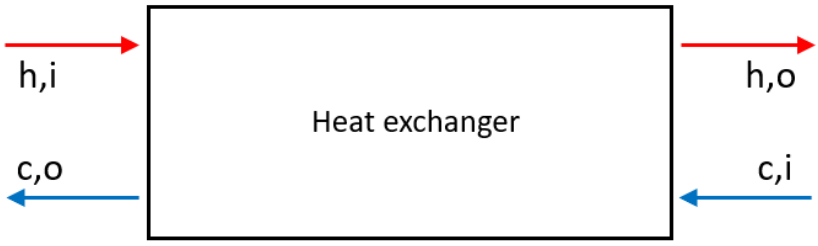

Figure 1.14: Physical model of a heat exchanger.

Mass balance

Under the assumption of having only one inlet and one outlet for the two fluids, the formulation of the mass balance equation is the following:

$$\begin{aligned} \dot{m}_{h,i} &= \dot{m}_{h,o} = \dot{m}_h \\ \dot{m}_{c,i} &= \dot{m}_{c,o} = \dot{m}_c \end{aligned} \tag{1.12}$$

where the indexes h and c stand for hot and cold, while i and o for inlet and outlet.

Energy balance

To write the energy balance equation, what has to be considered is the relationship be-

tween mass flow rate $\dot{m}$ and temperature T, related by the water specific heat c_p. The corresponding equation is here reported:

$$\dot{m}_h \cdot c_p \cdot T_{h,i} + \dot{m}_c \cdot c_p \cdot T_{c,i} = \dot{m}_h \cdot c_p \cdot T_{h,o} + \dot{m}_c \cdot c_p \cdot T_{c,o} \tag{1.13}$$

Naming $\dot{Q}_h$ and $\dot{Q}_c$ the two thermal powers exchanged, respectively, from the hot fluid and the cold fluid, one can obtain the following relations:

$$\begin{aligned} \dot{Q}_h &= \dot{m}_h \cdot c_p \cdot (T_{h,i} - T_{h,o}) \\ \dot{Q}_c &= \dot{m}_c \cdot c_p \cdot (T_{c,o} - T_{c,i}) \end{aligned} \tag{1.14}$$

Obviously, because of the energy balance between the hot and cold fluids, it results that:

$$\dot{Q}_h = \dot{Q}_c \tag{1.15}$$

Figure 1.15: A real heat exchanger of the Test Facility.

LMTD: Logarithmic mean temperature difference method

There are two possible methods for modeling an heat exchanger: the LMTD or the ε-NTU ("effectiveness-NTU"). In this case the Modelica simulator was developed implementing

the first one, which consists in the computation of the logarithmic mean temperature difference ΔT_{ML}. The heat exchanger model, according to this method, can be found by firstly considering an infinitesimal section dA of the heat exchange surface [29].

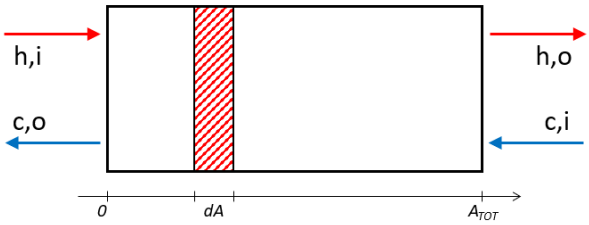

Figure 1.16: Physical model of a heat exchanger.

It's possible to write the infinitesimal thermal power exchanged between hot and cold fluid using the following relation:

$$\mid \delta\dot{Q}_h \mid = \delta\dot{Q}_c = \delta\dot{Q} = U \cdot dA \cdot (T_h - T_c) \tag{1.16}$$

where $\delta\dot{Q}$ is the infinitesimal thermal power exchanged in the infinitesimal area dA, T_h and T_c are the temperatures of the hot and cold fluid in the area dA, while U is the "global coefficient for thermal exchange". The latter is due to both the convective thermal exchange of the two fluids and the conductive thermal exchange of the heat exchanger; it has the following expression:

$$U = \frac{1}{\frac{1}{h_h} + \frac{1}{h_c} + \frac{s}{k}} \tag{1.17}$$

where h_h and h_c are the global coefficients for thermal exchange for the hot and cold fluid, s is the thickness of the wall and k is its thermal conductivity. Instead of taking into account only an infinitesimal section dA, now let's consider the whole surface A of the heat exchanger. In this case Equation (1.16) will be modified in the following way:

$$\dot{Q} = U \cdot A \cdot \Delta T_{ML} \tag{1.18}$$

where ΔT_{ML} stands for the logarithmic mean of the temperature difference ΔT and is computed as follows:

$$\Delta T_{ML} = \frac{\Delta T_2 - \Delta T_1}{\ln \frac{\Delta T_2}{\Delta T_1}} \tag{1.19}$$

A more detailed analysis of heat exchangers, as presented in "Corso di Termodinamica dei Processi di Conversione dell'Energia: Analisi Energetica ed Exergetica degli Scambiatori

di Calore" [29], could indeed provide further insights. However, this level of analysis is beyond the scope of this thesis, as the primary objective here is to simplify the model of each component to facilitate the design of a reduced model for Model Predictive Control. In Chapter 2 it will be explained how the heat exchangers are treated in the reduced model for MPC.

Chiller

The cooling system of the Facility is used to simulate the users requests in terms of absorbed amount of power; it is composed of four heat exchangers, a chiller, responsible of the water cooling and valves and a pump regulating the water mass flow and its pressure. Chiller (RR01) works taking as input the temperature setpoint which is desired at its outlet: this will be approximately the value of the water temperature entering every heat exchanger from the cold side of the network; we can assume this value around 10/15°C. After going through the heat exchangers, heated water follows the circuit and goes back to the chiller where it will be cooled and the cycle continues. The water flow is controlled by pump PR01, placed immediately after the chiller, and by four valves, which are also used to control the water temperature at the outlet of the heat exchangers in the hot side of the network, as will be explained in the following subsection. Chiller operates in stationary conditions, Equation (1.20), characterized by a pressure difference between inlet and outlet computed as in Equation (1.21). A photo of the real chiller is pictured in Figure 1.18, image taken from [24].

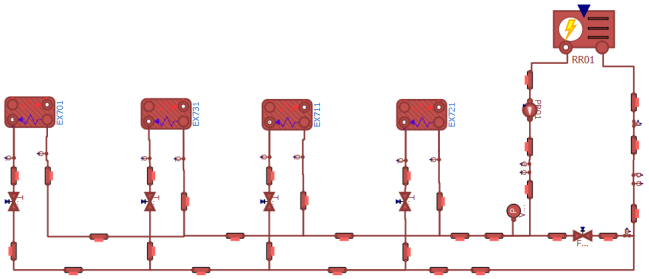

Figure 1.17: Cooling circuit of the Test Facility: four heat exchangers and the chiller.

$$\dot{m}_{in} = \dot{m}_{cold} = -\dot{m}_{out} \tag{1.20}$$

$$p_{in} - p_{out} = k_{cold}\dot{m}_{cold} \tag{1.21}$$

where k_{cold} is the pressure loss across the cold side (measured in $\frac{Pa}{kg/s}$). The amount of cooling power that this system can produce is 207 kW_{th}, as indicated in Table 1.1, which

follows the expression written in Equation (1.22).

$$P_{cold} = \dot{m}_{cold} \cdot (h_{in,cold} - h_{out,cold}) \tag{1.22}$$

Figure 1.18: Chiller of the RSE Test Facility.

Power control

In this subsection it will be explained how the power control is implemented in the real RSE Test Facility, making use of the controllable valves near the heat exchangers. Power control is useful because allows to impose a specific absorbed power profile to a heat exchanger, so that one is able to decide a priori the amount of power absorbed by the users. This is not so common in reality since what is normally done is to provide hot water at a certain supply temperature regardless of the amount of power a user consumes, but in this case the goal is to impose the power setpoint to see how the MPC will react and what it will decide in terms of supply temperatures and water mass flows. The power setpoint used in this thesis, reported in Figure 1.19, varies along one day: it can be seen that during the night the amount of requested power is very low, while its value increases during the day, particularly peaking in the morning.

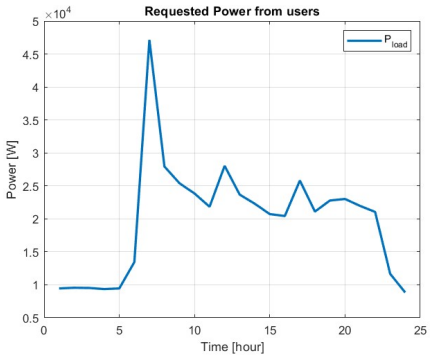

Figure 1.19: Profile of the power absorbed by users during one day.

Power control is realized along with a temperature control in order to impose both the power profile and the value of the return temperature, i.e. the water temperature exiting the heat exchangers. These controls are operated by two PID controllers for every heat exchanger; here we consider the heat exchanger EX701, but the discussion can be extended also to the others. The first PID controller, Figure 1.20, is used to regulate the return temperature: it takes as input the setpoint (in this case 65°C) and the measured return temperature, value given by the temperature sensor TT701. By continuously computing the difference between the setpoint and the measured temperature (i.e. the *error*), the PID controller acts on the valve TCV701, regulating the flow of water passing through it. In this way it is able to stabilize the return temperature to the value of 65°C.

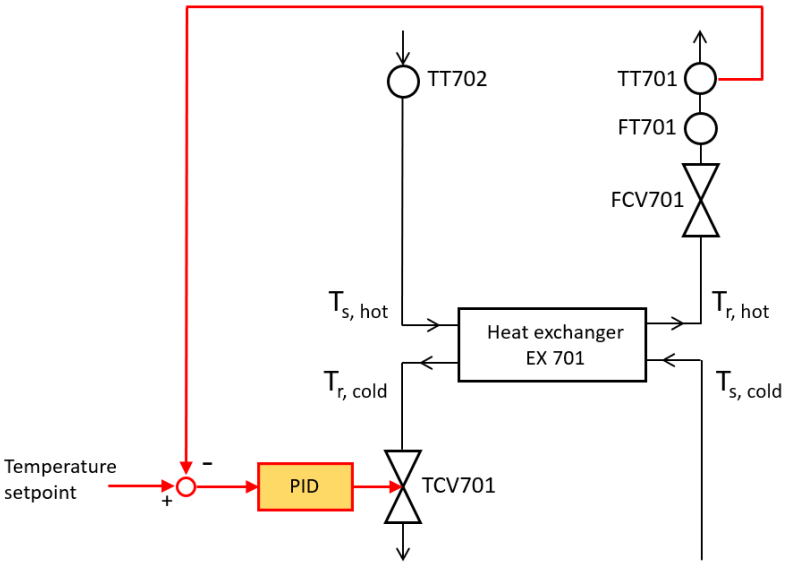

Figure 1.20: Scheme of the PID temperature control.

The other PID controller is used to impose the power profile. It operates following the scheme in Figure 1.21. This control scheme is divided in two parts: the first one concerns the computation of the mass flow setpoint to be given to the valve FCV701, the second one is the effective applied control action which uses the real measurement of the mass flow rate as feedback (from sensor FT701). The first block takes in input three values: the supply temperature measured by the sensor called "TT702", i.e. T_{TT702} , the return temperature setpoint and the power setpoint $P_{setpoint}$. Then, with a simple relation between these quantities, the mass flow rate setpoint is computed, as in Equation (1.23):

$$m_{setpoint} = \frac{P_{setpoint}}{c_p \cdot (T_{TT702} - T_{r,hot,setpoint})} \tag{1.23}$$

The output of the block, i.e. the water mass flow setpoint, then enters the PID control loop: using the real measurement of the water mass flow as negative feedback, PID acts on the valve FCV701 and is able to impose the desired power profile.

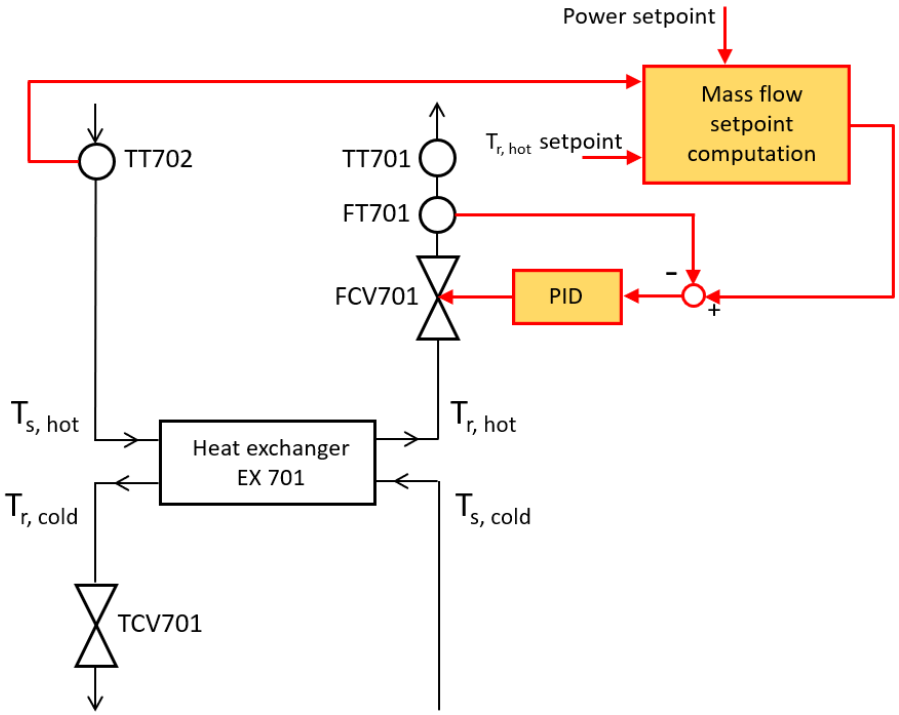

Figure 1.21: Scheme of the PID power control.

1.1.6. Pipes

Pipes in the RSE Test Facility have been dimensioned with a transmission line 200 m long, two distribution lines each 200 m long and four lines towards the users 25 m long (these values consider the supply network only). The transmission line is characterized by an internal diameter of 52.5 mm, a mass flow rate of 2.9 kg/s and a velocity of water passing through of 1.37 m/s. These values for the distribution lines and those ones to users become respectively: 35.1 mm and 26.6 mm the internal diameter, 1.45 kg/s and 0.72 kg/s the mass flow rate, 1.53 m/s and 1.33 m/s the velocity of water [30].

A DHN can be represented with a set of nodes, $\mathcal{N}$, and edges, $\mathcal{E}$, that are the physical interconnections among nodes [18]. Each node $i \in \mathcal{N}$ represents a significant element of the network, e.g. a thermal generator, a storage, a load etc. Edges are on the other hand the pipes of the DHN. They are modeled featuring the one-dimensional finite-volume

method [18]: it consists of the spatial discretization of the pipe in n mono-dimensional sections orthogonal to the water flow direction, as reported in Figure 1.22, where i and j stand for two different nodes of the DHN. y_{ij}^v represents the vertical displacement of the pipe, L_{ij}^v its length and r_{ij}^v and r_{ij}^{vm}, respectively, its internal and external radius. Every section of the pipe has a length of $l_{ij}^v = L_{ij}^v/n_{ij}^v$ and a volume $v_{ij}^v = l_{ij}^v \pi (r_{ij}^v)^2$.

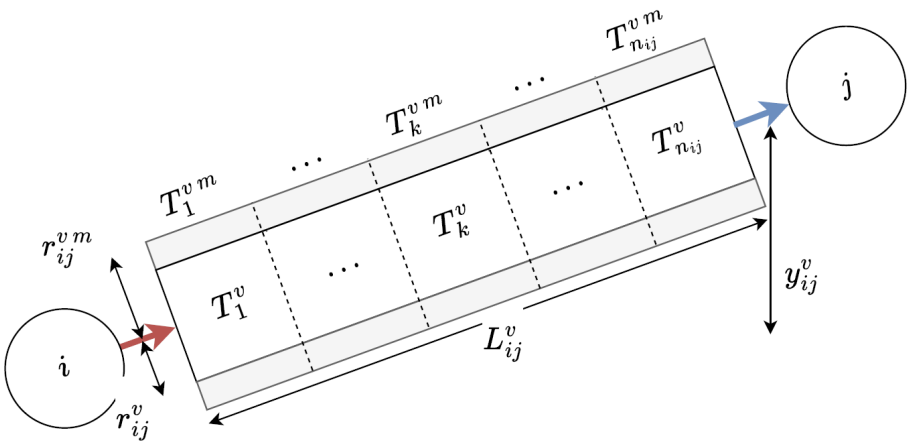

Figure 1.22: Discretization of the pipe in n sections (image taken from document [18]).

Considering a generic section of the pipe $k \in \{1, ..., n\}$, the first assumption to make is that there is no accumulation of flowing water; so it holds that $\dot{m}_k = \dot{m}_{k+1}$. Denoting with $T_{ij,k}^{vm}$ the temperature of the pipe wall of the k-th section and with $T_{ij,k}^v$ the water temperature, the dynamic model of the latter is:

$$\begin{aligned} c_p \rho v_{ij}^v \dot{T}_{ij,k}^v(t) = \; & 2\pi r_{ij}^v l_{ij}^v U_{ij}^m (T_{ij,k}^{vm}(t) - T_{ij,k}^v(t)) + \\ & + c_p q_{ij}^v(t) \begin{cases} T_{ij,k-1}^v(t) - T_{ij,k}^v(t) & if \quad q_{ij}^v(t) \geq 0 \\ T_{ij,k}^v(t) - T_{ij,k+1}^v(t) & if \quad q_{ij}^v(t) < 0 \end{cases} \end{aligned} \tag{1.24}$$

where ρ is the water density, U_{ij}^m the coefficient for thermal exchange between water and pipe walls and $q(t)$ is the flow rate of the pipe. Here is reported the dynamic model of the pipe metal wall temperature $T_{ij,k}^{vm}(t)$, which takes into account coefficient c_m (the parallel of c_p but related to pipe walls) and U_{ij}^e, the coefficient for thermal exchange towards the environment considered at temperature $T_{ij,k}^{v,e}(t)$:

$$c_m \rho_m v_{ij}^{vm} \dot{T}_{ij,k}^{vm}(t) = 2\pi r_{ij}^v l_{ij}^v U_{ij}^m (T_{ij,k}^v(t) - T_{ij,k}^{vm}(t)) - 2\pi r_{ij}^{vm} l_{ij}^v U_{ij}^e (T_{ij,k}^{vm}(t) - T_{ij,k}^{v,e}(t)) \tag{1.25}$$

Then, speaking about pressures, through the Fanning's formula, one can model the pressure drop across the pipe ($p_i^v(t) - p_j^v(t)$), as in Equation (1.26).

$$p_i^v(t) - p_j^v(t) = \rho g y_{ij}^v + \rho \begin{cases} c_f \frac{L_{ij}^v}{r_{ij}^v} \left(\frac{q_{ij}^v(t)}{\rho \pi (r_{ij}^v)^2} \right)^2 & if \quad q_{ij}^v(t) \geq 0 \\ -c_f \frac{L_{ij}^v}{r_{ij}^v} \left(\frac{q_{ij}^v(t)}{\rho \pi (r_{ij}^v)^2} \right)^2 & if \quad q_{ij}^v(t) < 0 \end{cases} \tag{1.26}$$

where c_f is the Fanning coefficient and g the gravitational acceleration. Finally, in Equation (1.27), is reported the expression for computing the pressure drop in case of a pipe fitting (intended as a lumped cross-section variation); according to Bernoulli's principle, the pressure drop at each pipe fitting edge (i, j) is:

$$p_i^v(t) - p_j^v(t) = \frac{(q_{ij}^v(t))^2}{2\rho} \begin{cases} k_{1,ij}^v & if \quad q_{ij}^v(t) \geq 0 \\ -k_{2,ij}^v & if \quad q_{ij}^v(t) < 0 \end{cases} \tag{1.27}$$

where $k_{1,ij}^v$ and $k_{2,ij}^v$ are fixed friction coefficients depending on the pipe fitting geometry (cross-section variation, contraction angles, etc). Further details can be read in the article [19], but as already explained the aim of this thesis is to simplify the DHN dynamics to design the computationally efficient model for MPC, which does not take into consideration pressures in the pipelines, as illustrated in Chapter 2.

1.2. Simulation Environment

Speaking about the used software, the modeling of the multi-energy system has been done into OpenModelica [20], an open source program developed by the Modelica association. The network model have been developed by RSE SpA in Modelica language, specifying all the values and equations related explained in the previous sections. A deeper analysis on how the simulator was realized has been done in document [19]. The MPC controller is instead created in Matlab and Simulink [16], software of Mathwork corporation, in Matlab language. The Modelica simulator has been used to validate the designed reduced model for MPC, checking whether it was able to accurate approximate the plant states behavior. Finally, the real tests on the RSE plant have been allowed by an interconnection between the Matlab MPC and a Python script directly connected with the Test Facility commands.

For the sake of example, here are reported a bunch of system states computed with the simulator. This water mass flow and temperature trends will be compared in Section 2.5 with results obtained from the reduced model for MPC. At the time of this simulation, the Modelica simulator didn't include CHP yet nor the power control, so in this case the plant was run using only gas boiler and electric boiler as heat generation. Here the settled reference temperature of gas boiler was a step from 74°C to 75°C, while that one of electric boiler followed a certain trajectory in the neighborhood of 70°C. Water mass flows through boilers were kept constant, 2.7 kg/s for gas boiler and 2.5 kg/s for electric boiler, as well as the by-pass valve. The simulation was conducted over a period of one day in order to observe the behavior of system, particularly al the heat exchangers.

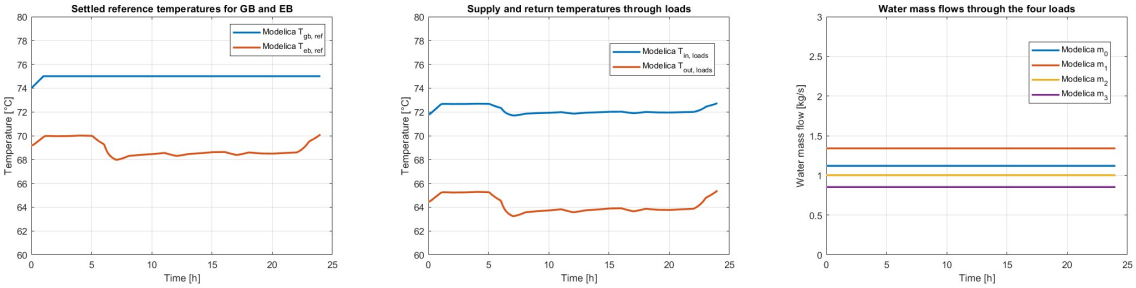

Figure 1.23: Results obtained from the Modelica simulator.

As can be seen in Figure 1.23, water temperature arriving to the heat exchangers is a sort of mean between the gas boiler outlet temperature and the electric boiler one: this is due to the water mixing in the network, phenomenon analyzed in Section 2.4.2. It can be observed that water arrives to each one of the loads at the same temperature, differently from the four mass flow rates, visible in the graph on the right, where there are some differences in terms of values.

1.3. Overall plant: RSE Test Facility

In conclusion, here the complete Test Facility plant introduced in Section 1.1.1 is presented with further details. In this picture, Figure 1.24, rectangles represent the pipelines that connect the various systems of the plant. One can see the heat generation section at the bottom, with water going to the primary pump P901 (in green on the left) through the centralized rack (the pipe system above the generators), the two storage tanks connected by a circuit of pumps and valves, and the section related to the users at the top, connected to the network through the distribution rack. On the right there's the by-pass valve, used to avoid an excessive water pressure in the network. Pumps and valves are used to control the water mass flow rate in every section of the plant, while one thing to be explained regards the CHP: it comprehends in fact also an heat exchanger ("E501") connecting it to rest of the network. In Section 2.4.4 it will be demonstrated that in the reduced model for MPC this heat exchanger can be neglected, without obtaining relevant differences in the model. In Table 1.1, there is a brief summary of the key data of the system. Here the detailed scheme of the primary network is depicted.

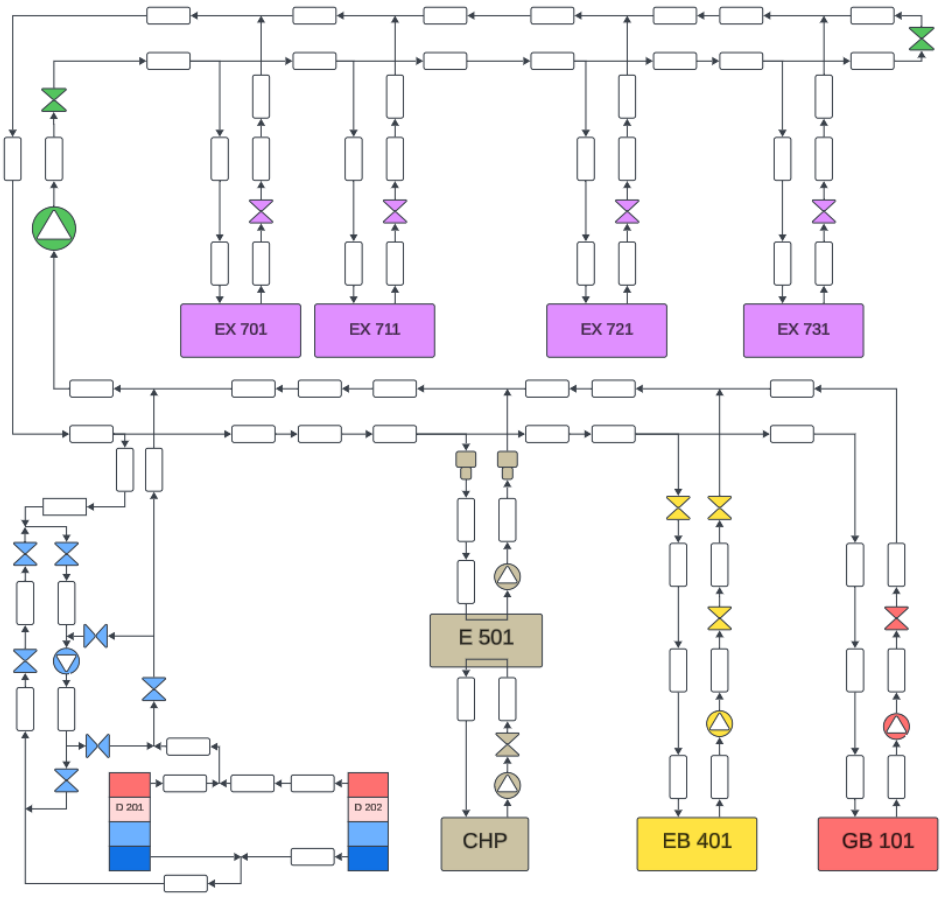

Figure 1.24: Whole primary network of the RSE Test Facility.

System	Enumeration	Principal component
Gas Boiler	100	• Thermal power: 147 kW_{th} (80/ 60°C)
Thermal Storage	200	• N° storages: 2 • Volume: 10 m^3
Electric Boiler	400	• Thermal power: 50 kW_{th} (80°C/60°C)
Co-generator CHP (Combined Heat and Power)	500	• Electrical power: 50 kW • Thermal power: 81 kW_{th}
Thermal loads (users)	700	• Thermal power: 50 kW_{th} (80/60 °C) • Electric heater: 10 kW
Rack Centralized/ Distributed and primary Pump	900	Primary pump and rack for connecting components in a centralized or distributed configuration (26 electro-pneumatic valves and 20 manual valves)
Rack Distribution	A00	Rack for connecting components to a distribution network (52 electro-pneumatic valves and 44 manual valves)
Cooling Circuit	R00	• Cooling power: 207 kW_{th}

Table 1.1: System components (table taken from document [24]).

2 | Model Predictive Control design and validation

In this chapter the reduced model for MPC is presented, showing the construction of every part of the plant in Matlab, along with its validation both in simulation, comparing the results with those obtained from OpenModelica, and in the real case with data obtained from experiments on the real RSE Test Facility.

2.1. MPC introduction

Model Predictive Control (MPC) is a sophisticated control strategy widely used in various industries for optimizing complex processes while satisfying constraints. It operates by continuously solving an optimization problem over a finite prediction horizon to determine the optimal control actions. This control approach has gained immense popularity due to its ability to handle multivariable systems, non-linearity, and constraints effectively. MPC was initially developed in the 1970s [15] but, over the years, it has evolved significantly, incorporating advanced optimization algorithms and computational techniques. Its practical success in diverse fields such as chemical, automotive, aerospace, and power systems has established it as the most popular advanced control method in industry.
The idea behind Model Predictive Control is that a predictive model captures the relationship between control inputs, system states, and outputs, and, by iteratively predicting future system behavior, a sequence of optimal control actions is computed over a finite time horizon. This sequence is then implemented over a shorter control horizon, and the process repeats at each time step. It's interesting to think how humans actually use an intuitive version of MPC in many aspects of their daily lives. An example is related to the game of chess: a good player tries to predict all the possible moves as far into the future as possible before making a move; then, the move he chooses is the one that he believes is the best one (optimal) given the prediction [21].

The formulation of the MPC control problem involves several key components:

- **Objective Function**: typically, a quadratic cost function is minimized, which balances the control objectives such as setpoint tracking, disturbance rejection, and energy consumption.
- **System Dynamics**: the predictive model describes how the system evolves over time in response to control inputs and disturbances. This model can range from simple linear models to complex nonlinear models.
- **Constraints**: MPC inherently handles both equality and inequality constraints on inputs, outputs, and states. Constraints ensure that the system operates within safe limits and operational constraints.

Designing an MPC controller involves selecting appropriate prediction and control horizons, tuning weighting factors in the cost function, and defining constraints. The choice of *prediction horizon* determines how far into the future the controller predicts, while the *control horizon* specifies the length of the control sequence applied at each time step. Proper selection of these parameters is crucial for achieving desired control performance. Implementing MPC requires solving an optimization problem at each time step, which can be computationally intensive, but, in general, this control scheme offers several advantages over traditional control strategies:

- **Multivariable Control**: MPC naturally handles systems with multiple inputs and outputs, enabling coordinated control of interconnected processes.
- **Constraint Handling**: it systematically incorporates constraints into the control formulation, ensuring safe and efficient operation even in the presence of disturbances.
- **Robustness**: the predictive nature of MPC allows it to adapt to changes in the system dynamics and disturbances, enhancing robustness and performance.

2.2. Optimization Solver

Considering the time horizon T and a number N of discrete time steps, each one of this steps is an optimization problem to be solved. Therefore, a solver connected to the Matlab software is needed: the choice has fallen on CasADi, an open source software which also integrates the IPOPT package (useful when taking into account large-scale nonlinear optimization problems).

2.3. Discretization

Since this thesis concerns a dynamic optimization problem, to find a solution all the dynamic equations describing it have to be discretized. In general, an equation expressed in discrete time takes the form:

$$x_{k+1} = f(x_k, u_k)$$

A good choice for the discretization of differential equations is the Euler Backward method which allows to compute how a generic function $y(t)$ evolves through time given its mathematical expression and an initial condition:

$$\frac{dy}{dt} = f(t, y)$$

$$y(t = 0) = y_0$$

To derive the algorithm, recall the backward difference approximation:

$$\frac{dy}{dt} \approx \frac{y_k - y_{k-1}}{\tau}$$

Now, equaling the expression of the derivative of y with its approximation and shifting the whole equation forward in time by one step (i.e. replacing k by $k+1$ everywhere), one gets:

$$\frac{y_{k+1} - y_k}{\tau} = f(t_{k+1}, y_{k+1})$$

The Euler Backward method is finally derived by making y_{k+1} explicit:

$$y_{k+1} = y_k + \tau f(t_{k+1}, y_{k+1})$$

2.4. MPC reduced modeling

In this section, all the elements of the Test Facility presented in Chapter 1 are modeled one by one in the Matlab reduced model and, in case of Sections 2.4.1 and 2.4.4, validated singularly using the Modelica simulator (libraries *DHN4Control* and *MultiEnergySystem*). In particular, as stated in the introduction, the objective is to build a control-oriented reduced model that neglects irrelevant dynamics of the system, in order to have a less computationally demanding regulator capable anyway to represent in a satisfactory way the

system itself. In particular, as illustrated in details in document [19], the simplifications that are here made are:

- fixed direction of the working fluid;
- load model reduction: load control is assumed to track the output reference temperature from heat exchangers correctly, as explained in Section 1.1.5;
- pressures of the fluid are not considered: since pressures are not directly related to the economic management of DHNs (economic cost function illustrated in Section 2.7), they can be excluded from the NMPC problem. This allows for a great simplification on the whole model of the MPC, guaranteeing a very reduced computational effort for the solver.
- water flows through the TES in only one direction at a time, see Section 2.4.6.

Taking into account these considerations, the MPC problem is defined as a Nonlinear Model Predictive Control (NMPC) and its general formulation is reported in Equation (2.1):

$$min_{x,u} \quad J \tag{2.1}$$

$$\begin{aligned} \text{s.t.} \quad & x(k+1) = f(x(k), u(k)), \;\; k = 0, \ldots, N \\ & X(0) = X_0 \\ & U_{min} \leq U(k) \leq U_{max} \\ & X_{min} \leq X(k) \leq X_{max} \end{aligned}$$

where constraints taken into account are respectively: the most relevant dynamical equations governing the plant, the initial values of the state X_0 and the physical limitations for states X and inputs U. Inputs are, in particular, the outlet temperature of gas boiler and electric boiler, the electrical power of CHP, the water mass flow rates passing through each of these generators and that of the primary pump. If also the thermal storage is included in the NMPC problem, there are two additional control actions: the water flow charging or discharging the tank. Additionally, some state constraints included slack variables to ensure feasibility.
The cost function J to be minimized is reported and explained in Section 2.7, while constraints are illustrated in the following subsections.

2.4.1. Pipes

In the reduced model for MPC, a pipe is modeled through a Matlab function called *"addPipe"*, which uses the Euler Backward method presented in Section 2.3 to implement equations of Section 1.1.6. As already explained, the main objective is to reduce the complexity of the model neglecting irrelevant dynamics and so for this reasons Equations (1.26) and (1.27) are not considered. This function allows to create a generic pipe of certain length and diameter, divided in a given number of sections according to the theory explained in Section 1.1.6, with settable initial temperature of all the sections to a desired value. Then, based on the value of the incoming flow rate of water, the temperature behavior in the pipeline is calculated taking into account the amount of heat lost to the environment, Q_{amb}. This parameter depends on the external surface of the pipe, on the temperature difference between water and ambient and also on a constant U computed as follows:

$$U = \frac{2\pi\lambda_{insulation}}{\log \frac{r_{ext}}{r_{int}}} \tag{2.2}$$

where r_{ext} and r_{int} are the external and the internal radius of the pipe, respectively. In figure 2.1 there's an example of how *addPipe* works: the left image represents the temperature behavior of a pipe in the supply network (initialized at 65 °C and with a certain incoming water flow rate at 82.5 °C), while the right one is a pipe in the return network (hence maintained at 65 °C). Both pipes have a generic value for length and diameter, 5 m and 5 cm respectively, and are divided in two sections. The simulation has been conduced over a period of one day.

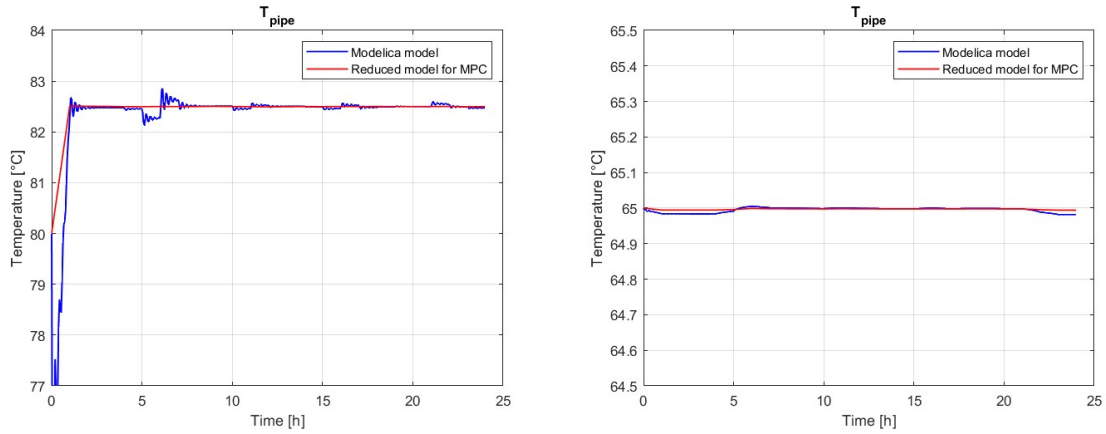

Figure 2.1: Temperature behavior of a supply pipe (on the left) and of a return pipe (on the right).

In addition to showing the temperature trend in the two sections of the pipeline (red and yellow lines), the graph also displays the one calculated using the model of a pipe in Modelica (blue line). As one can see the behavior computed with the reduced model for MPC approximates quite well the one simulated with OpenModelica: this is also certified by the Key Performance Indexes "NMBE" and "CVRMSE", which express the accuracy of the obtained graphs, and are computed as follows:

$$\begin{aligned} NMBE(\%) &= \frac{\sum(x-\hat{x})}{N\bar{x}} \cdot 100 \\ CVRMSE(\%) &= \frac{\sqrt{\frac{\sum(x-\hat{x})^2}{N-1}}}{\bar{x}} \cdot 100 \end{aligned} \tag{2.3}$$

where x is the value obtained from Modelica, $\hat{x}$ from the MPC model, $\bar{x}$ is the mean of x and N is the prediction horizon. The MPC model can be considered satisfactory enough if NMBE is less than 10% and CVRMSE is less than 30%. The graph of the supply pipe has NMBE equal to 0.02526% and CVRMSE to 0.1105%, while the return line indexes are 0.00168% and 0.00683% respectively. Hence, the MPC reduced model representing the temperature in a pipeline can be considered accurate.

2.4.2. Mixing temperature

This subsection concerns the computation of the temperature mixing equation describing the behavior of the water temperature in the nodes, where water of different temperatures is mixed. This situation is expressed in Figure 2.2: two incoming flow rates m_1 and m_2 at different temperatures T_1 and T_2 are mixed together in a resulting flow rate m_{out} (sum of the two) at temperature T_{out}.

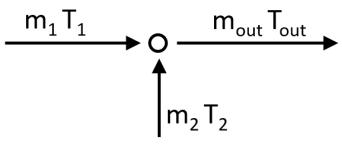

Figure 2.2: A generic node where two flow rates at different temperatures interact.

$$T_{out} = \frac{m_1 T_1 + m_2 T_2}{m_1 + m_2} \tag{2.4}$$

In a Matlab function called *"temperatureMix"* the resulting temperature is computed at

every time instant as in Equation (2.4). This function is used every time there's the need to represent an intersection of pipelines in the Test Facility.

2.4.3. Gas Boiler and Electric Boiler

The MPC reduced models for gas boiler and electric boiler are quite similar and deal with the power (from gas or electricity) used by these machines to set the desired water temperature in output and satisfy the users needs. Power is constrained by the actual construction limits of the machines and can thus vary within the range represented by these values. In Equation (2.5) and (2.6) are reported the expressions of gas boiler and electric boiler powers that are used by the MPC to compute the optimal control action, i.e. the optimal outcoming water temperature $T_{gb,out}$ or $T_{eb,out}$, given the incoming water temperatures $T_{gb,in}$ and $T_{eb,in}$ and the incoming flow rates m_{gb} and m_{eb}. The boilers' efficiencies are also considered, being represented by η_{gb}, with the value of 0.82, ans η_{eb}, equal to 0.95. ${T_{gb,out}}^{\min}$ and ${T_{gb,out}}^{\max}$ are set to 75°C and 90°C, respectively (the same for the electric boiler).

$$\begin{cases} {P_{gb}}^{\min} \leq P_{gb} \leq {P_{gb}}^{\max} \\ P_{gb} = \frac{m_{gb} \cdot c_p \cdot (T_{gb,out} - T_{gb,in})}{\eta_{gb}} \\ {T_{gb,out}}^{\min} \leq T_{gb,out} \leq {T_{gb,out}}^{\max} \end{cases} \tag{2.5}$$

$$\begin{cases} {P_{eb}}^{\min} \leq P_{eb} \leq {P_{eb}}^{\max} \\ P_{eb} = \frac{m_{eb} \cdot c_p \cdot (T_{eb,out} - T_{eb,in})}{\eta_{eb}} \\ {T_{eb,out}}^{\min} \leq T_{eb,out} \leq {T_{eb,out}}^{\max} \end{cases} \tag{2.6}$$

2.4.4. CHP: circuit model reduction

In this subsection is illustrated how the co-generator is taken into account in the reduced model for MPC. First of all, it's important to say that the Combined Heat and Power has been realized by implementing a small simplification to reduce the computational effort on the solver. As one can see in Figure 2.3, the complete CHP includes an heat exchanger and hence an additional little network: this means that the solver has to deal with a bunch of variables which represents the exchange of power between mass flow rates m_{chp1} and m_{chp}. In this subsection it's shown how these variables could be removed from the MPC model, obtaining anyway almost the same results (the difference is not too large

and so acceptable) and simplifying a little the whole problem. To reach this goal, a little experimental network with only CHP and a user, see Figure 2.3, has been settled up, but this idea can be brought to the real situation, substituting the user in this little DHN with the rest of the real Test Facility network.

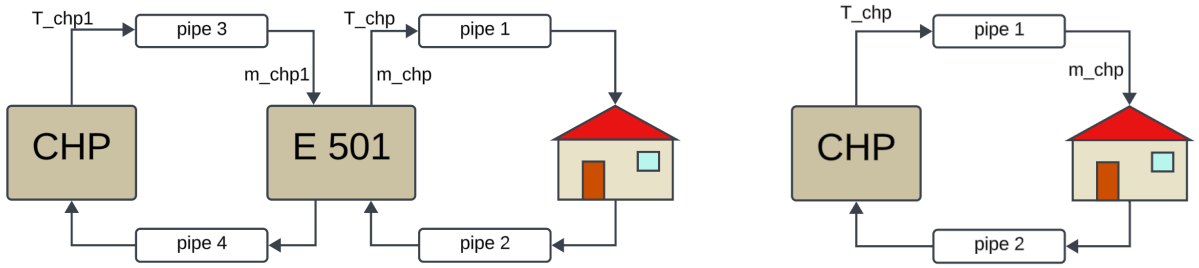

Figure 2.3: Little experimental district heating network with CHP and user (the house): on the left the complete CHP model, on the right the simplified one.

Two MPC models have been settled up, one representing the complete network and the other the simplified one. Results are expressed in Figures 2.4: for simplicity, only the most meaningful graph are reported (electrical and thermal power and the graph of the temperature behavior in pipe 1). The goal is to show that dashed lines (values of the complete network) can be approximated by the solid ones (values of the simplified network); thus, the simplified MPC model for the CHP can be used in place of the complete one.
In Equation (2.7) are reported the expressions describing the CHP that are used by the MPC to compute the optimal control action, i.e. the optimal electrical reference power $P_{chp,elec,ref}$, related to thermal power by the efficiencies η_{elec} (0.4193) and η_{th} (0.5453). The electrical power setpoint is computed based on the water mass flow and the outgoing temperature needed to satisfy the users power consumption.

$$\begin{cases} {P_{chp,elec}}^{\min} \leq P_{chp,elec,ref} \leq {P_{chp,elec}}^{\max} \\ {P_{chp,th}}^{\min} \leq P_{chp,th} \leq {P_{chp,th}}^{\max} \\ P_{chp,th} = \frac{P_{chp,elec,ref}}{\eta_{elec}} \eta_{th} \\ P_{chp,th} = m_{chp} \cdot c_p \cdot (T_{chp,out} - T_{chp,in}) \\ {T_{chp,out}}^{\min} \leq T_{chp,out} \leq {T_{chp,out}}^{\max} \end{cases} \tag{2.7}$$

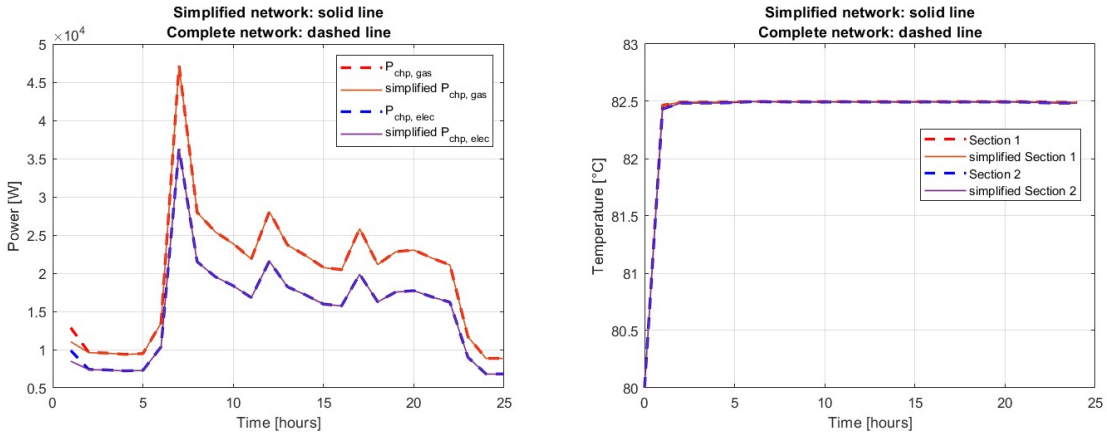

Figure 2.4: Comparison between complete network (dashed lines) and simplified network (solid lines). On the left both electrical and thermal powers, on the right the temperature behavior of water in pipe 1 (the one towards users).

2.4.5. Thermal exchange at the loads

Following the concepts stated in Section 1.1.5, here is illustrated how the thermal power exchanged in the loads, between hot and cold water, is modeled in the Model Predictive Control script. The reduced model for MPC makes a great simplifications of the equations, with respect to the Modelica simulator, since the only dynamic constraint taken into account is reported in Equation (2.8). This means that for each load i, the MPC model considers the settled absorbed power $P_{setpoint,i}$ (varying at each sampling time) and computes the mass flow rate m_i and the ingoing water temperature $T_{in,i}$, minimizing the cost function. The return temperature value is kept constant at the reference $T_{out,ref,i}$, e.g. 60°C, because of the implementation of the PID temperature control, see Section 1.1.5. c_p is the water specific heat.

$$m_i \cdot c_p \cdot (T_{in,i} - T_{out,ref,i}) = P_{setpoint,i} \tag{2.8}$$

2.4.6. Thermal Storage

The thermal storage is modeled in the MPC with a Matlab function called *"addTank"* which allows to represent the behavior of water temperature in TES according to Euler Backward method, Section 2.3, and to the theory illustrated in Section 1.1.3. Through *addTank* it is possible to create a generic tank of certain dimensions and compute its temperature trend based on the charge and discharge water flow rates passing along the pipes connecting it to the network. These flow rates are calculated by the MPC to fulfill the network's demands while considering energy costs: this allows the tank to be charged during the most cost-efficient times of the day, and to discharge it (and so utilize the stored energy) when the network requires it most. The reduced MPC model of the thermal storage doesn't include the power lost towards the environment due to temperature difference, since the whole tank is well insulated and hence this value can be considered negligible. In Figure 2.5 one can see how *addTank* works: it is reported an example of a tank, dimensioned exactly equal to the real RSE TES and divided in four layers, charged continuously with a water flow rate of 2.7 $\frac{l}{min}$ (0.77 $\frac{kg}{s}$) at 43°C. Starting temperature is around 25°C. The graph shows also the comparison with the same thermal storage, using four layers, simulated in Modelica through the library *MultiEnergySystem*.

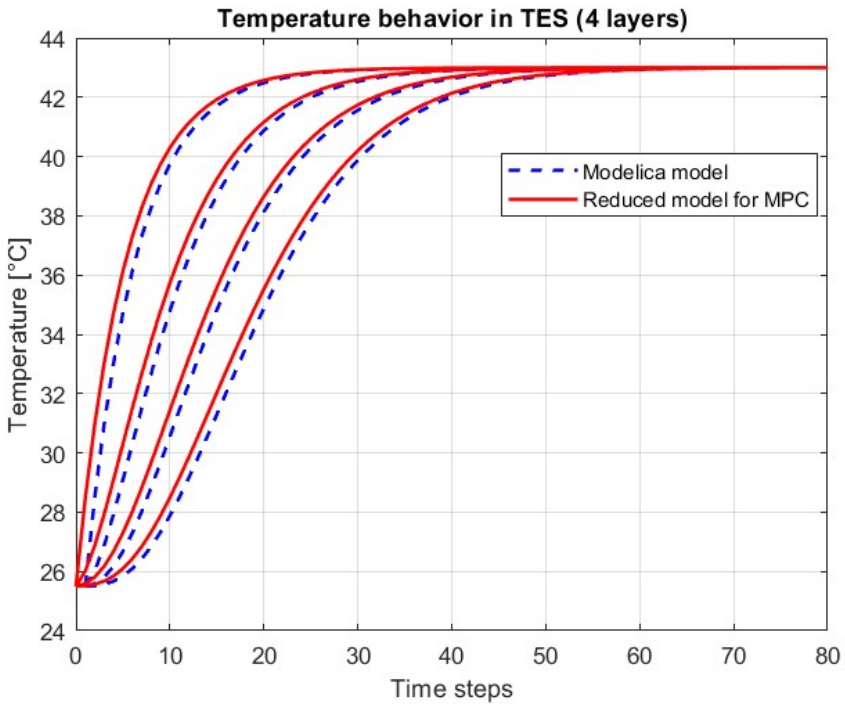

Figure 2.5: Comparison between a four layers tank computed with the MPC reduced model (using a sampling time of 600 seconds) ad the one simulated with Modelica.

The picture shows that the MPC tank model is able to approximate the Modelica model in a quite satisfactory way, as expressed also by the Key Performance Indexes: $NMBE = 3.241066\% < 10\%$, $CVRMSE = 2.432735\% < 30\%$. Anyway, one aspect to be particularly taken into account is the choice of the number of layers to divide the component in; in fact, this significantly influences the settling time of the temperature. In Figure 2.6 there is the comparison between the same tank as before divided into ten layers and fifty layers computed with the MPC model using again 600 seconds as sampling time.

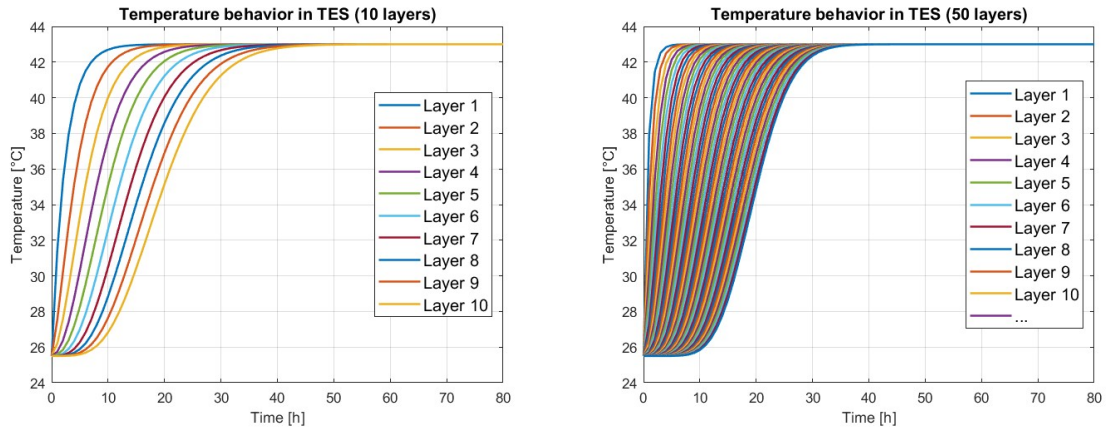

Figure 2.6: Same tank divided in a different number of layers. It's possible to see the variation in the settling time: the more the layers, the less is the settling time and the real situation could be approximated better.

As can be deduced, the desired value of the layers number could be idealistically a large number, but this would obviously lead to a considerable computational effort for the solver. On the other hand, a too small value could create discrepancies between the model and the real RSE TES temperature behavior. Experimental data demonstrate that about ten layers can represent the behavior in a satisfactory way without significantly affecting the resolution time. As an example, in Figure 2.7 it's reported a validation with real data obtained from the real RSE thermal storage, put in the same condition in terms of starting temperature and charging water flow as the modeled one. Since the real TES has four sensors to measure its internal temperature, the MPC model has been run using fifty layers to approximate correctly the behavior, but showing only four of them (those located in correspondence with the actual sensors).
To conclude the discussion regarding the design of the reduced model for TES, the constraints applied in the Model Predictive Control are reported in Equation (2.9). The first aims at considering the water passing through the tank only at one direction at a time, as explained in Section 2.4. Hence, at every time instant only one among m_{charge} and $m_{discharge}$ can be different from zero. The second, instead, concerns the maximum and

minimum water temperature inside the TES itself, $T_{TES,i}{}^{\min}$ and $T_{TES,i}{}^{\max}$, considering every layer.

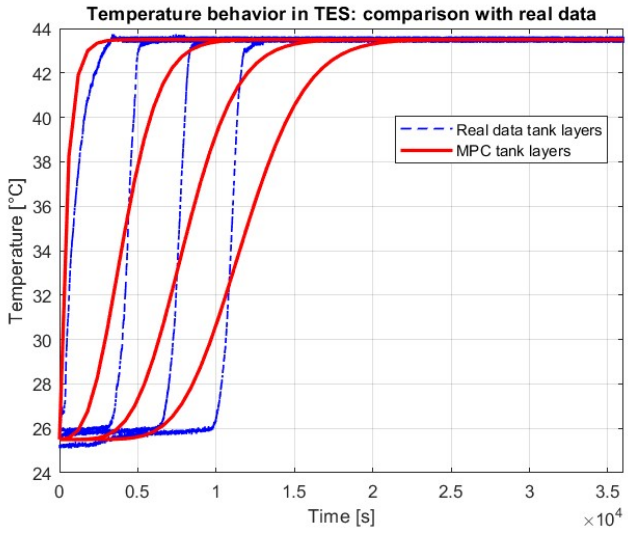

Figure 2.7: Model validation with real data. If the number of layers in the MPC model were further increased and the sampling time decreased, the real trend would be approximated even more accurately.

$$\begin{cases} m_{charge} \cdot m_{discharge} = 0 \\ T_{TES,i}{}^{\min} \leq T_{TES,i} \leq T_{TES,i}{}^{\max} \qquad for \;\; i = 1...n_{layers} \end{cases} \tag{2.9}$$

2.5. Reduced model Validation in simulation

In this section the complete reduced model for MPC is checked in order to see if it represents correctly the dynamics of the system: hence results are compared to those one obtained from the Modelica simulator developed by RSE, as already explained in Section 1.2. At the time of this test the simulator didn't include CHP yet, so in this case validation is performed regarding a plant with only gas boiler and electric boiler as heat generation; anyway, a complete verification comprising the CHP is realized using real data in Section 2.6.

The idea was to give the same input data (in terms of reference temperature for gas and electric boiler, absorbed power from users, return temperatures from heat exchangers etc.) to both the Modelica simulator and the Matlab MPC and see if the predicted states of the reduced model have a correct behavior. As illustrated in Section 1.2, in this test the settled reference temperature of gas boiler is a step from 74°C to 75°C, while that one of electric boiler follows a certain trajectory in the neighborhood of 70°C. Water mass flows through boilers are kept almost constant and also the one in the by-pass valve. In the following pictures results are presented: not all the system states are shown, but only some of them (the most representative ones). Graphs are generated over the course of a day, choosing a sampling time equal to one hour. First, in Figures 2.8 and 2.9 are reported, respectively, the behaviors of the supply and return temperatures to the distribution rack, i.e. temperatures in pipelines measured by sensors TT901 and TT902, and the return temperatures of gas and electric boilers. Then, in Figure 2.10 some other important states are checked: water mass flows through heat exchangers and through the by-pass valve, which are not settled and hence not known a priori.

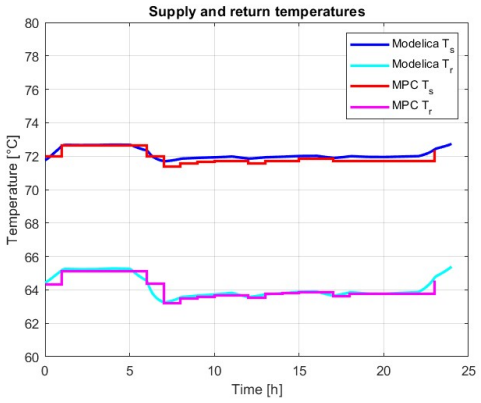

Figure 2.8: Validation using Modelica simulator of the supply and return temperatures to the distribution network, T_s and T_r. States predicted by the reduced model match quite well the ones computed with OpenModelica.

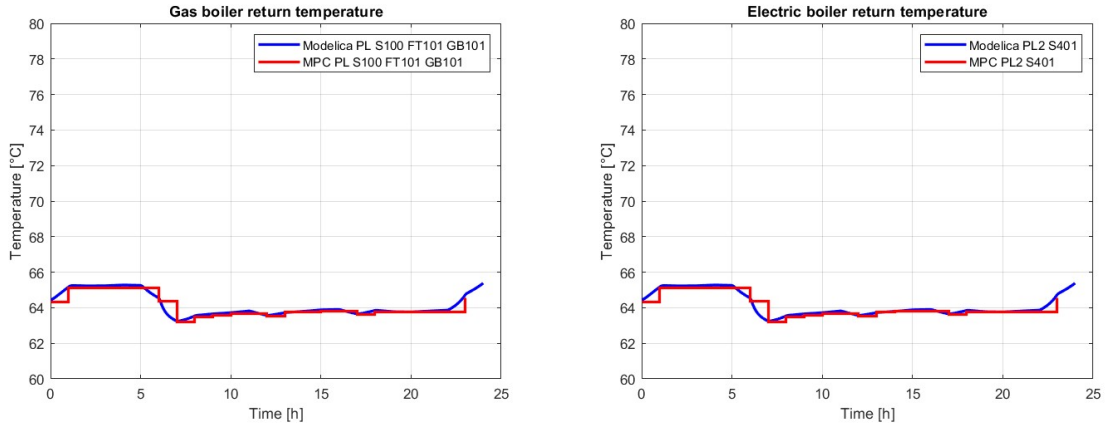

Figure 2.9: Validation using Modelica simulator of the temperature of water going back to gas boiler (a) and to electric boiler (b).

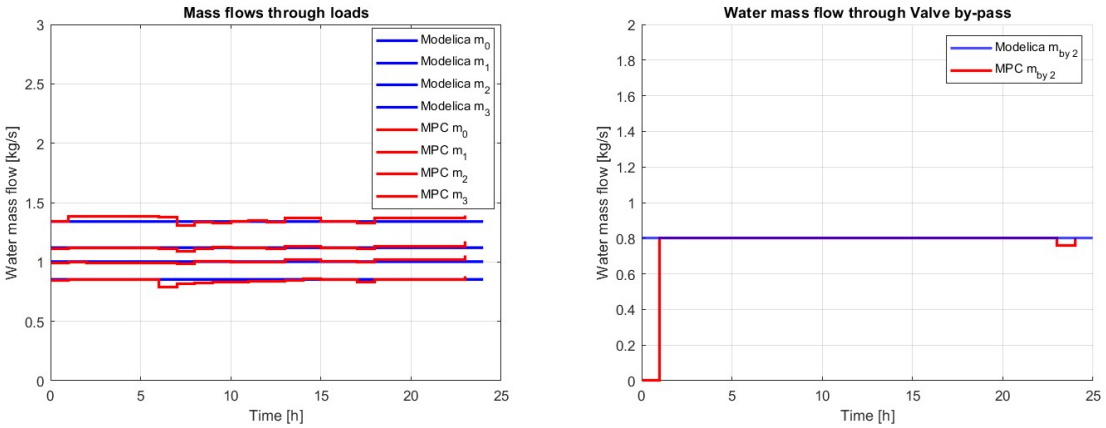

Figure 2.10: Validation using Modelica simulator of the water mass flows through every heat exchanger (a) and through the by-pass valve (b).

It can be seen that the reduced predictive model for MPC is able to approximate well the system states computed with the Modelica simulator, even neglecting some dynamics such as the pressure differences. For a further comparison here below are six graphs representing some system water temperatures taken as a sample for the validation. Pipelines checked here are: *"rackCD Hot SXXX SYYY"* and *"rackCD Cold S900 S200"* (supply and return temperatures in rack centralized), *"rackL3L4 FCVC01 hot"* and *"FCVC01 rackL4L5 cold"* (supply and return tempeatures in rack distribution between heat exchangers EX711 and EX721), *"rackL6L7 FCVC02 hot"* (temperature of water through the by-pass valve), *"Pl701 TT702 SourceIn"* (supply temperature of heat exchanger EX701; results of the other heat exchangers are not reported being similar).

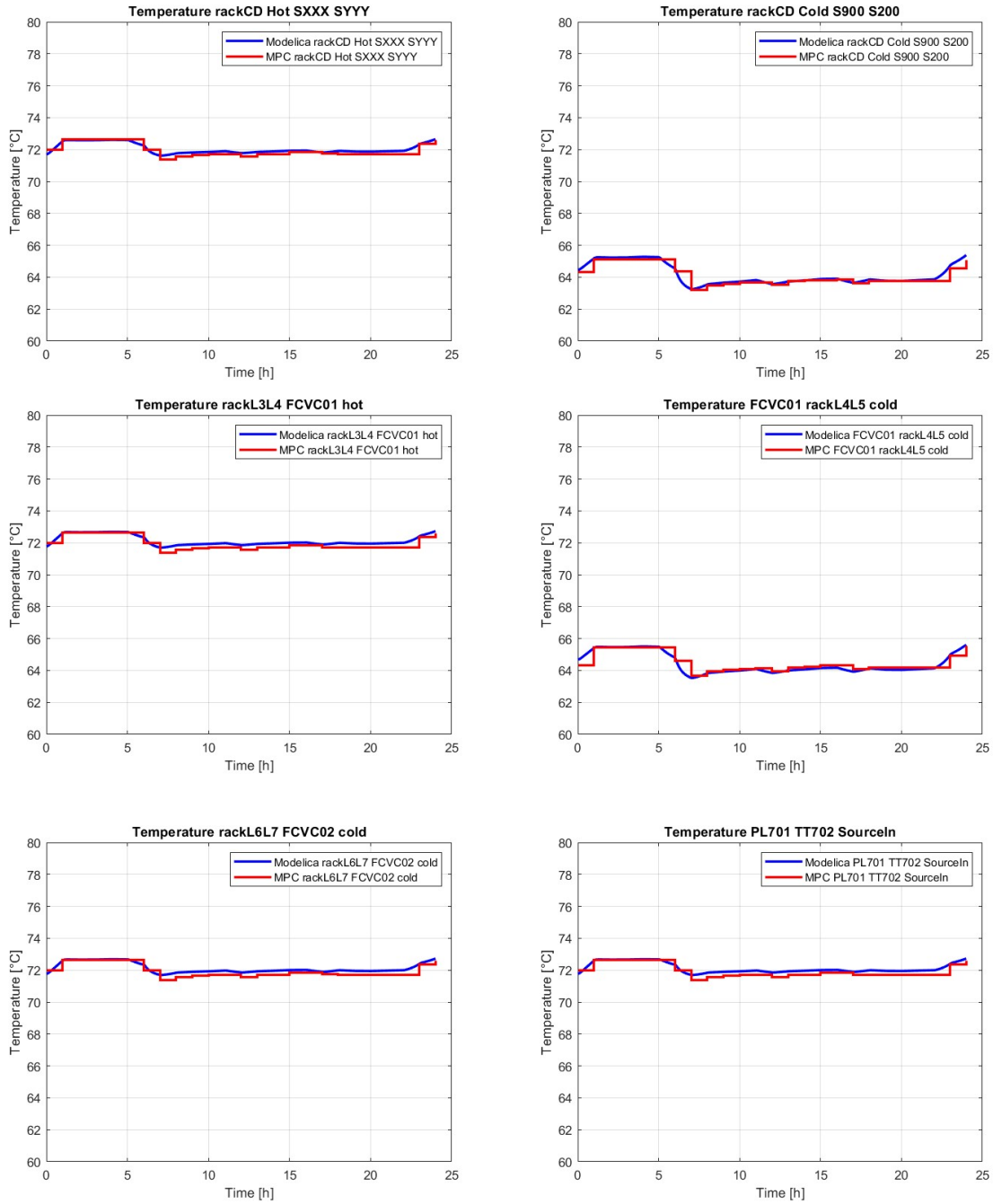

Figure 2.11: Validation using Modelica simulator of some system states taken as a sample.

2.6. Reduced model Validation with real data

In this section is reported the validation of the reduced model for MPC with real data obtained from the RSE Test Facility. The test has been operated giving the same input values to the plant and to the control-oriented model and collecting measurements from the sensors to be compared with the simulated ones. First, the Test Facility has been brought to a water temperature of 70°C for the supply lines and 60°C for the return ones; then, a step on the setpoint temperatures of gas boiler and electric boilers (respectively, 77°C and 76°C) has been applied in order to monitor the evolution of the system. The CHP output temperature has been instead kept constant at 70°C, as well as its water mass flow, kept at 3.5 $\frac{l}{min}$ (around 0.95 $\frac{kg}{s}$). Water mass flow through electric boiler has been given a step setpoint, varying its value from 4 to 2.5 $\frac{l}{min}$ (i.e. from 1.1 to 0.69 $\frac{kg}{s}$). The gas boiler water flow has been used as the free one so as to make the network able to absorb the desired power with the heat exchangers. Finally, the by-pass valve has been taken closed (not completely since there's a minimum opening surface for safety).
The model has been given exactly the same inputs and the same values of power absorbed from the heat exchangers. Since the real test had a duration of around four hours, it has been decided to simulate the model with a sampling time of 900 seconds and a prediction horizon equal to fifteen steps. One aspect to consider is that the reduced model was modified slightly because, in reviewing these tests, it became evident that power losses to the environment are significantly higher than those in simulation. This is demonstrated by the supply temperature profiles of the heat exchangers, where the temperature decreases much more than in the simulation. This discrepancy is due to real-world losses along the network that are not accounted for in the simulation. Therefore, an additional coefficient was introduced in the reduced model for the MPC, representing power losses, with a different value for each pipe to better match the real measurements and accurately reflect the actual system behavior.
Keeping in mind these considerations, results of the predictions made by the reduced model are reported here below. As observed for the validation in simulation, Section 2.5, the predicted states match the actual measures in a satisfactory way. Some differences have been noticed regarding water temperature in the return pipelines towards boilers. The reason comes from a bunch of valves of the thermal storages which cannot be fully closed and this created an undesired mixing of water which is not considered by the MPC model.

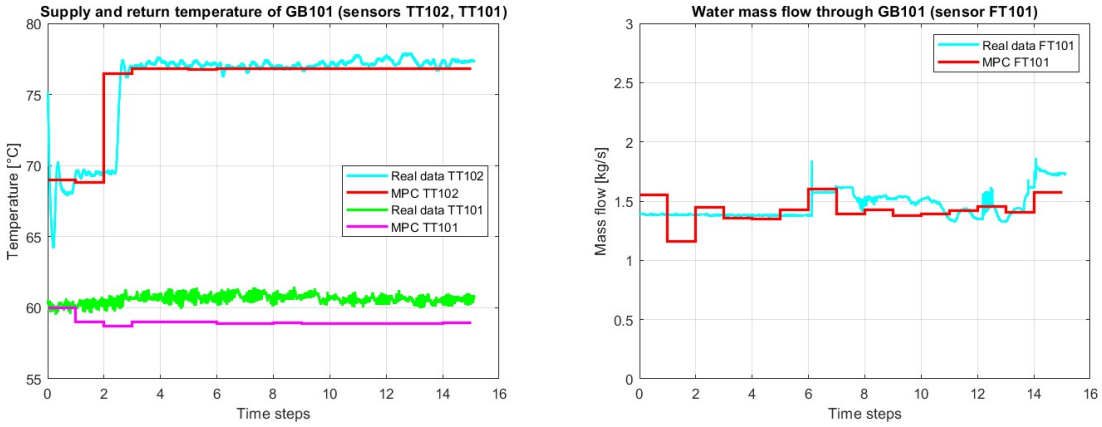

Figure 2.12: Validation with real data of gas boiler supply/return temperature (a) and water flow (b). It has been observed that the return temperature does not precisely match the actual measured value. This discrepancy arises because the MPC model calculates the behavior of the return pipes starting from an initial value of 60°C, which then decreases due to heat losses to the environment. As said, the Test Facility includes on the other hand some undesired mixing of water from the tanks, which could not be completely stopped and generates this difference.

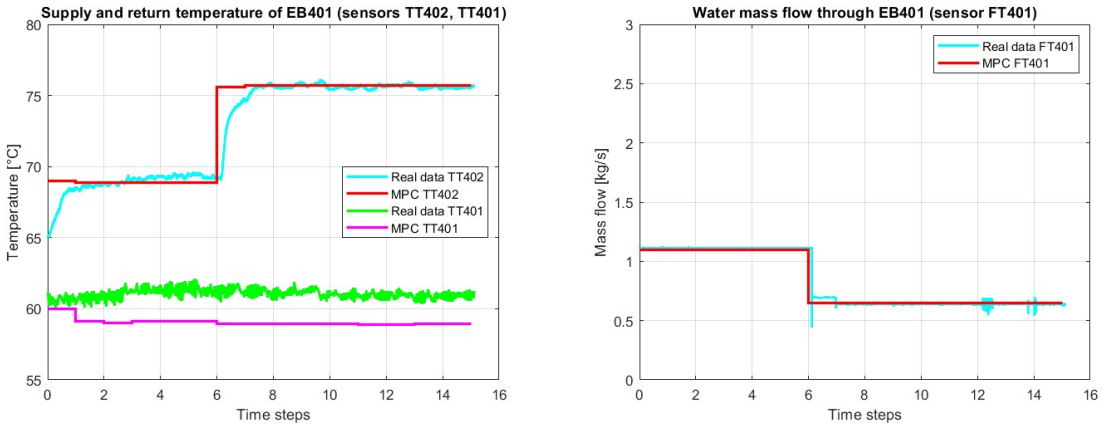

Figure 2.13: Validation with real data: electric boiler supply/return temperature (a) and water flow (b).

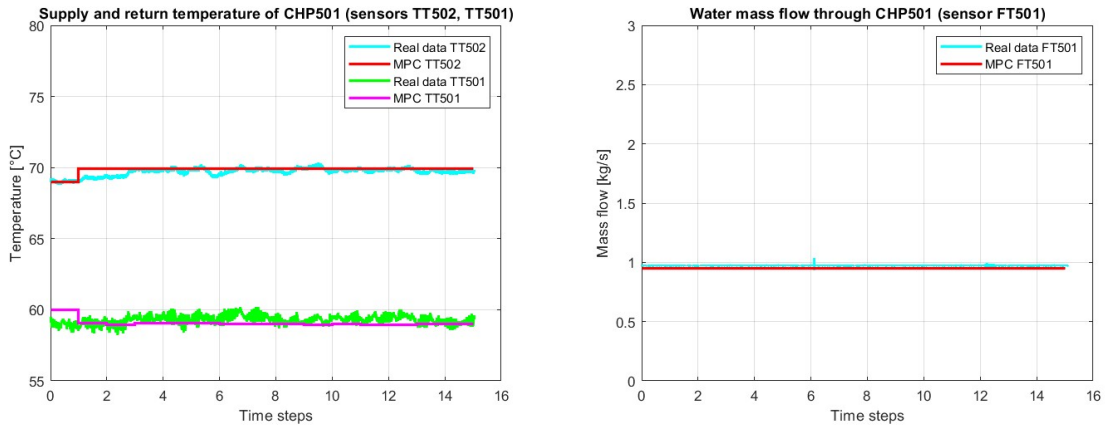

Figure 2.14: Validation with real data:CHP supply/return temperature (a) and water flow (b).

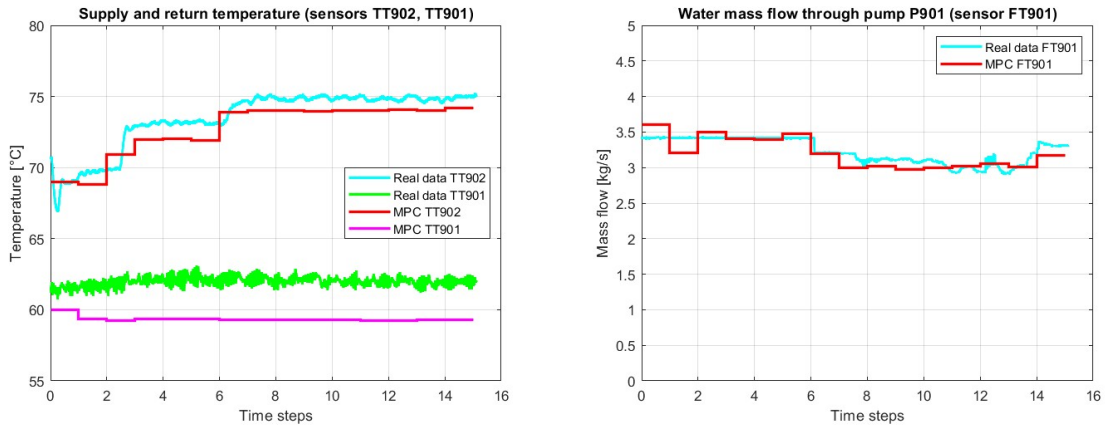

Figure 2.15: Validation with real data of pump P901 boiler supply/return temperature (a) and water flow (b).

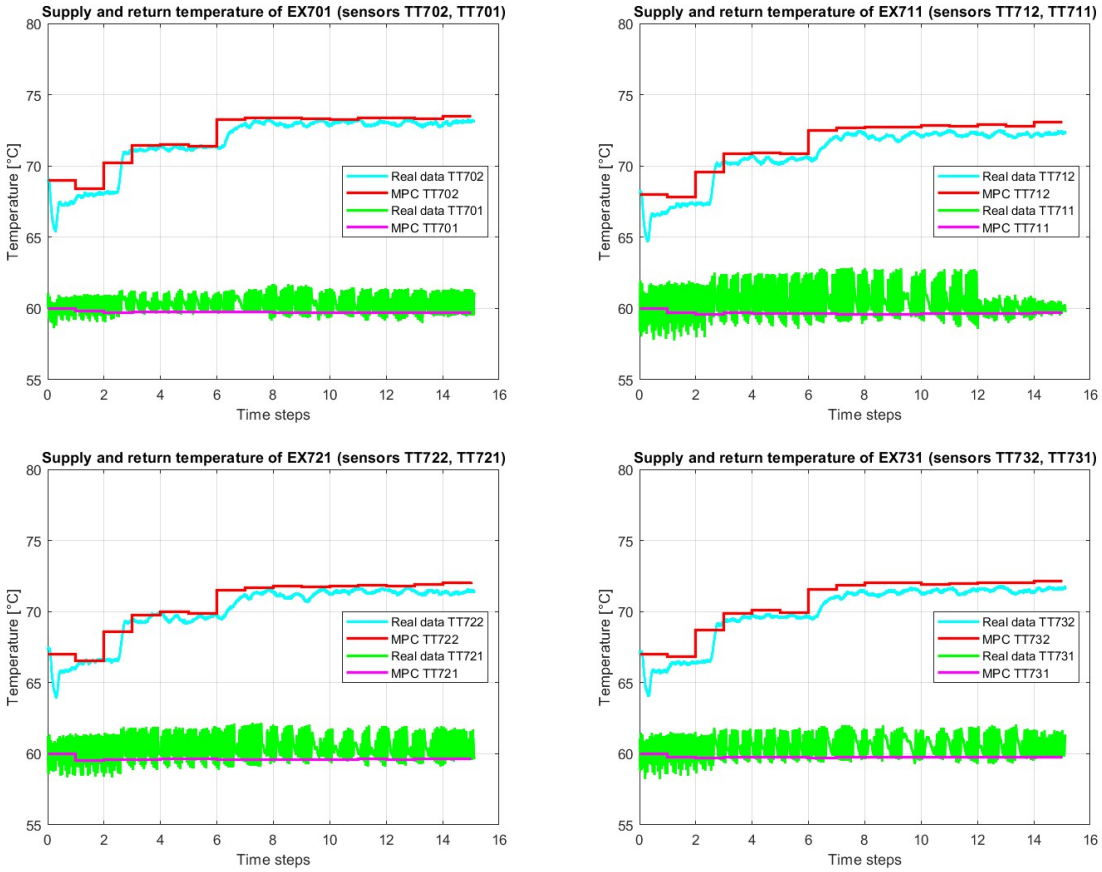

Figure 2.16: Validation with real data of heat exchangers supply and return temperatures. The observable oscillations of the green graph (real data return temperature) are due to the PID temperature control; the reduced MPC model does not include these oscillations (purple graph).

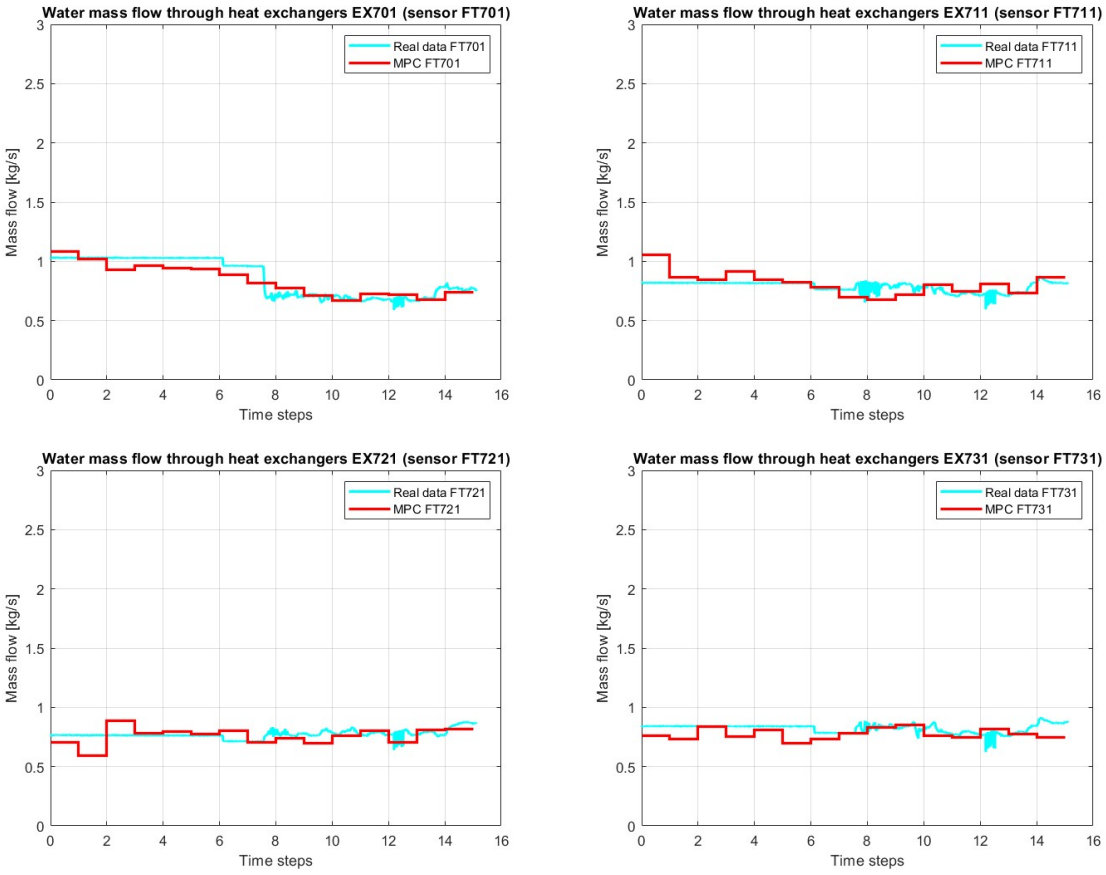

Figure 2.17: Validation with real data of heat exchangers water flow rates.

2.7. Cost Function

The MPC optimal control problem has been stated in Equation (2.1) and it's focused on the minimization of a suitable cost function J while respecting constraints. The choice of the cost function is a key point to run the MPC. In literature is shown that the most common objective functions for optimization problems in DHNs and MESs are the economical ones, concerning energy production costs, eventual curtailments and units operational costs [17]. For this reason the cost of natural gas C_{gas} and that one of electricity C_{elec} have been taken into account, varying throughout the day. The implemented cost function is a combination between economical terms and others related to the plant. For example the value of water mass flow passing through the by-pass valve, named m_{by}, is penalized, since the goal is primarily to meet the users need and so what is desirable is that the MPC finds a solution where the water in the by-pass is minimized. In Equation (2.10) the expression of the objective function J is reported:

$$\begin{aligned} J \;=\; & \sum_{k=0}^{N+1} P_{gb,\,gas} \cdot C_{gas} \\ & + \sum_{k=0}^{N+1} P_{eb,\,elec} \cdot C_{elec} \\ & + \sum_{k=0}^{N+1} P_{chp,\,gas} \cdot (C_{gas} - \eta_{elec} \cdot C_{elec}) \\ & + \sum_{k=0}^{N+1} \alpha \cdot m_{by} \end{aligned} \tag{2.10}$$

where $P_{gb,\,gas}$, $P_{eb,\,elec}$ and $P_{chp,\,gas}$ are respectively the thermal power produced by gas boiler, the electrical power of electric boiler and the thermal power of CHP, η_{elec} the electrical efficiency of the latter and α is a coefficient used to weight the by-pass flow rate term of the cost function. In this case $\alpha = 100$. The third row of Equation (2.10), in particular, takes that form since it concerns the minimization of the power consumption of CHP ($P_{chp,gas} \cdot C_{gas}$), but meanwhile subtracting the electrical power sold ($P_{chp,gas} \cdot \eta_{elec} \cdot C_{gas}$).

If thermal storage is also considered in the plant, a related term should be added to the cost function. One possible approach is to minimize the quadratic difference between the TES temperature at the end of the prediction horizon and a specified threshold $T_{TES,threshold}$, such as 80°C, as expressed in Equation (**??**). Anyway, during tests on the real plant, thermal storage was not considered, thus the implemented cost function was the one in

Equation (2.10).

$$J_{TES} = J + (T_{TES,threshold} - T_{TES,i}(N+1))^2 \qquad for\ \ i = 1, ..., n_{layers} \tag{2.11}$$

2.8. State constraints

Speaking about constraints, the MPC involved the whole dynamical reduced model illustrated in section 2.4, along with those reported in Equations (2.5), (2.6), (2.7), (2.8), (2.9), in order to work in the range of feasibility of the Test Facility not overcoming physical limitations in terms of water temperature and power production. In particular, outlet water temperature of generators was set in the range between 70°C and 80°C, except for the CHP which had a maximum water temperature of 70°C. Furthermore, minimum and maximum physical limitations regarding water mass flows through pipelines were considered: respectively, 0.75 $\frac{kg}{s}$ and 1.2 $\frac{kg}{s}$ for electric boiler, 0.4 $\frac{kg}{s}$ and 1 $\frac{kg}{s}$ for CHP, while gas boiler mass flow was free to vary until a maximum of around 2 $\frac{kg}{s}$. One constraint was then related to the water flow through the by-pass valve m_{by}, which was kept almost at the zero value using a slack variable to ensure feasibility for the solver. Additionally, a constraint related to the minimum water temperature arriving at heat exchangers was added to ensure a minimum loads water temperature; its value was set depending on the cases. Finally, if also the TES was considered, a state constraint for limiting the internal water temperature was considered: minimum and maximum values were set to 60°C and 80°C respectively.

2.9. Running MPC online in simulation

Before implementing the MPC regulator on the actual plant, it was first tested in simulation using MATLAB Simulink. Constraints were prepared with their actual value for the Test Facility, the absorbed power profile imposed to the loads maintained almost the same trend of that in Figure 1.19, picking in the morning and then decreasing, but adjusting its values to have no issues with the physical RSE heat exchangers: the minimum was thus set to 25 kW and the maximum to 47 kW. Every load absorbed the same power. Costs of gas and electricity varied in the range between 0.2 \$/kWh and 0.7 \$/kWh, as can be seen in Figure 2.18. Thermal storage was considered even if during real tests was not taken into account; the tank was divided in four layers. Minimum and maximum outlet temperatures of generators were set to 70°C and 80°C, respectively. The state constraint of

having a minimum supply water temperature for loads was considered, setting this value to 75°C. Simulation was conducted over a period of one day using one hour as sampling time.

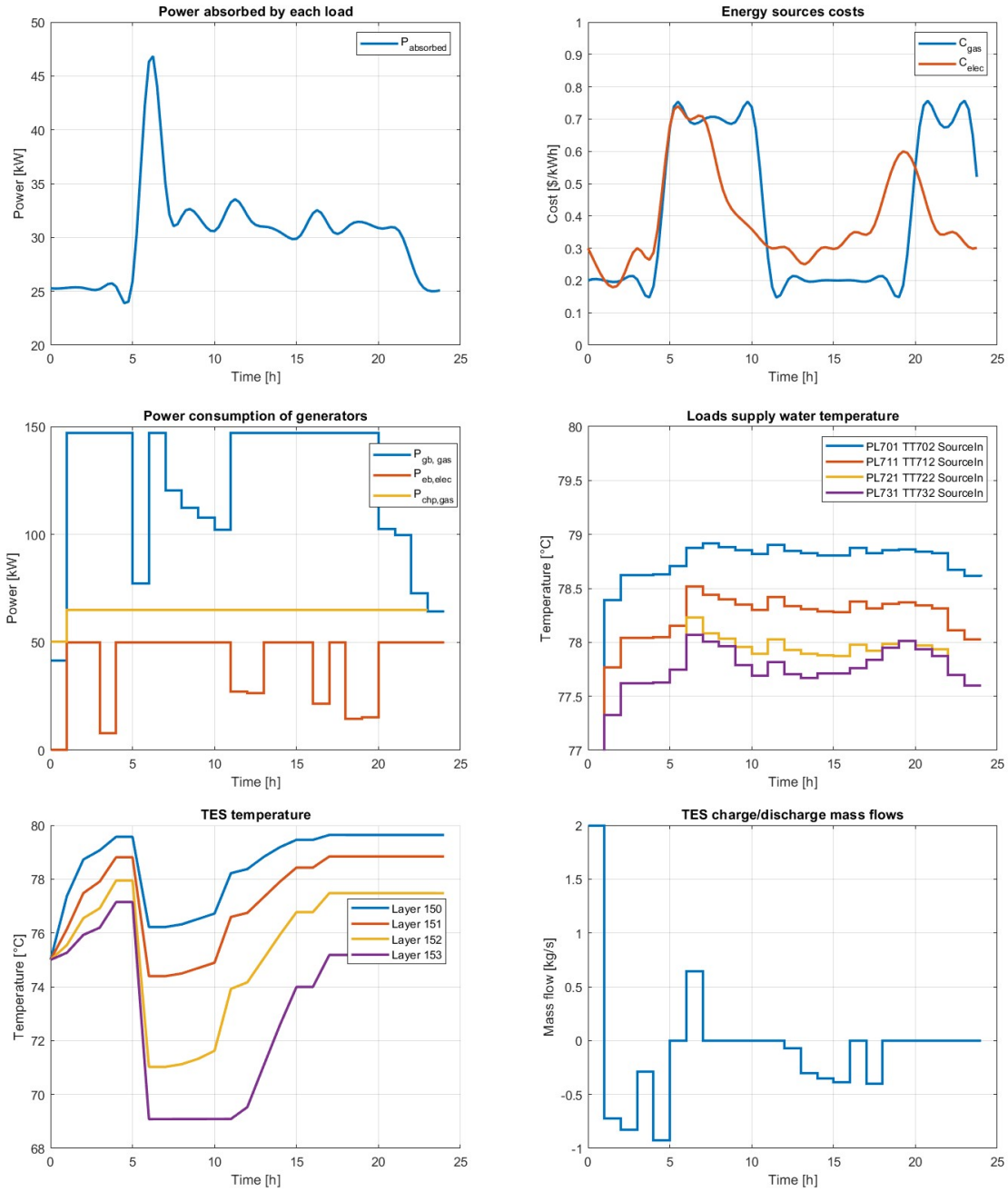

Figure 2.18: MPC simulation results: absorbed power profile for each load (a), cost of gas and electricity (b), generators powers consumption (c), inlet water temperature for loads (d), internal water temperature of TES (e), TES mass flow charge/discharge (f).

It can be seen from the graphs that generators are used always almost at the maximum

power given the high environmental losses across the network, except for some moments of day in which it's more economically convenient to operate in a different way. In particular, Model Predictive Control is able to pre-charge the thermal storage and pipes in prevision of periods of need. In Figure 2.18 (e) it's reported the behavior of the internal temperature of TES, filling it with heated water in the morning, before the pick of high power demand from loads. After that MPC decides to discharge it to bring heated water directly to the users. In the last part of the day TES is charged again since the MPC aims at keeping its temperature around 75°C at the end of the prediction horizon, following Equation (2.11), and this is done in the most economically convenient moment.
Finally, these results from MPC were compared to results obtained from the same network, but operated in such a way to keep generators powers and outlet temperatures almost constant (anyway satisfying loads constraints at the same time) and removing the thermal storage, in order to check the benefit of a Model Predictive Control regulation in terms of economical costs. Figure 2.19 displays the trend of the two cost functions (blue one is the one related to the DHN regulated by the MPC, red one is the one of the same DHN operated with the second strategy) during the whole day. One can see that effectively an MPC algorithm allows to maintain reduced costs with respect to normal DHNs by making its decisions in advance, for example the pre-charging of TES.

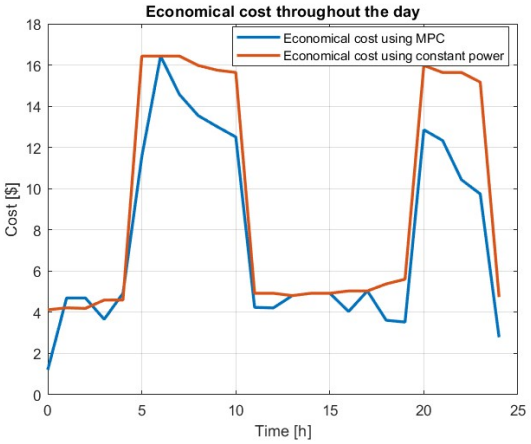

Figure 2.19: Cost comparison: cost functions of the DHN regulated by MPC (blue graph) or with the second control strategy (red graph).

Additionally, the exact percentage of cost savings was calculated by comparing the total costs of the two strategies shown in Figure 2.19. The calculated cost saving of 15.96 % demonstrates the advantages of the MPC algorithm over the second strategy.
In conclusion, some tests checking how the MPC regulator behaved were conducted in simulation using Matlab Simulink. When it comes to experiments on the real plant, instead, some other issues have to be taken into account. The most important one is to

know the actual values of the system states at every time instants. This is the objective of Chapter 3, where it will be explained how this challenge is tackled, designing a state estimator: the Moving Horizon Estimator.

3 | Moving Horizon Estimation design and validation

In this chapter, the addressed topic is related to the value of the network states at each sampling instant, i.e. water flow rates and their respective temperatures. In fact, the RSE Test Facility is equipped with numerous sensors for flow rate, temperature, and pressure (the latter, however, is not considered in the reduced model for MPC), but they are not sufficient to measure all the network states (e.g. temperature at each pipe section). This is why a discussion regarding the development of a state estimator is of fundamental importance: in this thesis, the choice has fallen on a Moving Horizon Estimator, which allows for the estimation of those states of a system that are not measurable, through the minimization of a suitable cost function based on the available measurements.

3.1. Moving Horizon Estimation

As mentioned in the chapter introduction, Moving Horizon Estimation is an optimization-based state-estimation technique where the current state of the system is inferred based on a finite sequence of past measurements; in many ways it can be seen as the counterpart to model predictive control (MPC). In comparison to more traditional state-estimation methods, e.g. the Extended Kalman Filter (EKF), MHE will often outperform the former in terms of estimation accuracy. This is especially true for non-linear dynamical systems, which are treated rigorously in MHE and where the EKF is known to work reliably only if the system is almost linear during updates [14]. Another advantage of MHE is the possible incorporation of further constraints on estimated variables [14]; all this, of course, at the cost of greater computational effort.

The basic idea of MHE is that the current state of the system is computed based on the dynamical model and a sequence of the past N measurements, where N is referred to the length of the horizon window. This is formulated as an optimization problem, where the finite sequence of states, algebraic states and inputs are optimization variables. These

sequences are determined, such that: the initial state of the sequence is coherent with the previous estimate, the computed measurements match the true measurements and the dynamic state equation is obeyed [14]. This nonlinear programming (NLP) problem is formulated at each sample time when a batch of new measurements is introduced and the states are estimated simultaneously [11] (iteratively, the new measurements are taken into account, while those further back in time are discarded).

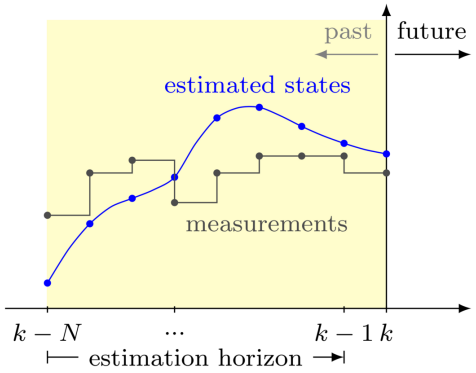

Figure 3.1: Graphic explanation of Moving Horizon Estimator (image taken from [8].

In the considered case study, the sensors measurements used in the state estimator are listed here below, grouped by subsystem:

- **Gas boiler:** supply and return temperatures, water mass flow. Sensors TT101, TT102, FT101.
- **Electric boiler:** supply and return temperatures, water mass flow. Sensors TT401, TT402, FT401.
- **Pump P901:** supply and return temperatures, water mass flow. Sensors TT901, TT902, FT901.
- **By-pass valve:** water mass flow. Sensor FTA12: valve closed except for its minimum physical opening area.
- **Heat exchangers:** supply and return temperatures, water mass flows. Sensors TT701, TT702, FT701, TT711, TT712, FT711, TT721, TT722, FT721, TT731, TT732, FT731.

3.2. MHE initialization

MHE works by taking as input two matrices: the first one is a 22xN matrix (being 22 the sensors used) collecting the last N measurements from sensors, while the other is a 7xN matrix (since 7 is the number of control actions) collecting the past MPC "u". The logic of the developed estimator is that, before running it online, they must be initialized with reasonable values; since before applying any control action the plant has to be brought in temperature, the matrices are filled with steady-state values (for example, 70°C and 60°C for supply and return temperatures). Then, at each MHE iteration, the first column (representing the oldest measurements) is discarded, and a new data column vector is appended at the end. This way, the two matrices consistently maintain the correct dimensions and always contain the most recent measurements.

3.3. Cost Function

Following the approach of the previous sections, the MHE optimization problem is formulated as the minimization of a cost function J, which is expressed in Equation 3.1. The solver has to find a solution that respects the same dynamic constraints used in the reduced MPC model, except that here the absorbed power by the heat exchangers is not considered. Instead, the model relies only on temperature and water flow measurements from the plant.

$$\begin{aligned} J \;=\;& \alpha \sum_{i=1}^{m}\sum_{k=0}^{N} \left(x_i(k) - x_i{}^{\text{meas}}(k)\right)^2 \\ &+ \beta \sum_{i=1}^{n} \left(x_{0,\,i} - \tilde{x_{0,\,i}}\right)^2 \\ &+ \gamma \sum_{i=1}^{p}\sum_{k=0}^{N} \left(u_i(k) - u_{prec,\,i}(k)\right)^2 \end{aligned} \tag{3.1}$$

The written cost function concerns the time steps k from 0 to N, where N represents the present time and 0 the furthest past instant. Indexes m, n and p stand for the number of measurable states, unmeasurable states and inputs, respectively. The first term of the cost function is related to the minimization of the quadratic difference between the measurable state variables and their actual measurement obtained from the sensor during the whole horizon window. The second term concerns the minimization of the difference between the initialization value (x_0) of the unmeasurable states and the value at step $k = 2$ ($\tilde{x_0}$) of the correspondent variables in the previous iteration of MHE: in this way

it's possible to initialize correctly the states at every iteration. Lastly, the third term is used to ensure that the control actions variables are as close as possible to the values of their respective variables output from the MPC (u_{prec}), in order to compute the estimate of the states based on the past inputs calculated from the MPC. Turning now to α, β, and γ, these represent the weights assigned to the terms in the cost function to achieve the best possible state estimation.

3.4. MHE validation in simulation

In this section the Moving Horizon Estimator is tested using the Modelica simulator, as done for the MPC reduced model in Section 2.5. Measurements have been collected from OpenModelica and given as input to the MHE, along with a suitable matrix containing the control actions "u". Results are expressed in Figure 3.2, where a bunch of significant graphs are displayed: it can be seen that the estimator satisfactorily approximates the measurements from the plant. A more detailed validation is realized in the following section using real data. Obviously, measurements have to be discretized, so MHE follows the correct profile, but keeping the values constant during the sampling interval. Here the simulation has been carried out during a whole day using a sampling time of one hour.

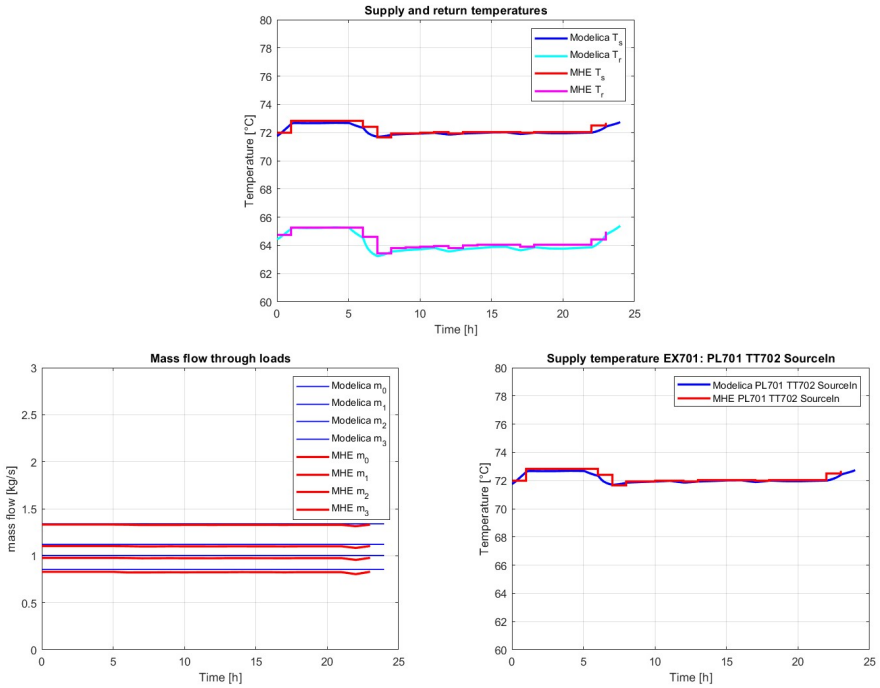

Figure 3.2: Supply and return temperature to the distribution rack (above), water flows and temperature arriving to loads (below).

3.5. MHE validation with real data

In this section the Moving Horizon Estimator is validated with real data collected from the Test Facility, those ones used also in Section 2.6, checking whether it can accurately estimate the system states. Similarly to what has been done with simulation data, MHE took as input measurements from sensors and a matrix collecting the applied control actions (for example a step temperature setpoint as reference of the boilers). Validation has been carried out in a way that simulates a real test on the plant: MHE matrices were initialized with steady-state values and, at each iteration, older data were discarded to make room for new ones. It is also important to point out that the "u" matrix contained the actual setpoints sent to the plant: in fact, the water flow references were correctly followed, while, for some reason, the boilers' outlet temperature setpoints were not perfectly reached. For instance, in the case of gas boiler, the reference was a step from 70°C at steady state to 80°C, but the outlet temperature read by sensor TT102 was around 77°C. One of the advantages of MHE compared to other observers is precisely its capability to overcome this drawback, as it weighs input data in its cost function in order to provide the best possible estimate of the system state, consistently with its dynamics. Hence, the expected behavior is that MHE is able to compute the dynamic of both measurable and non-measurable system states based only on the measurable ones. A sampling time of 900 seconds was chosen to cover the entire four-hours data collection period. Results are expressed in Figures from 3.3 to 3.5.
One aspect to clear is the real data discretization. In fact, at every iteration, MHE considers the measures from the sensors constant for the whole sampling interval. Hence, every time it is called, it minimizes the difference with the values that, for example in Figure 3.3, are highlighted with blue dots. This aspect is more evident in the temperature graph (figure (a)). Discrepancies in the return temperatures that are visible in the figures are due to the reasons already explained in Section 2.6 Figure 2.12.

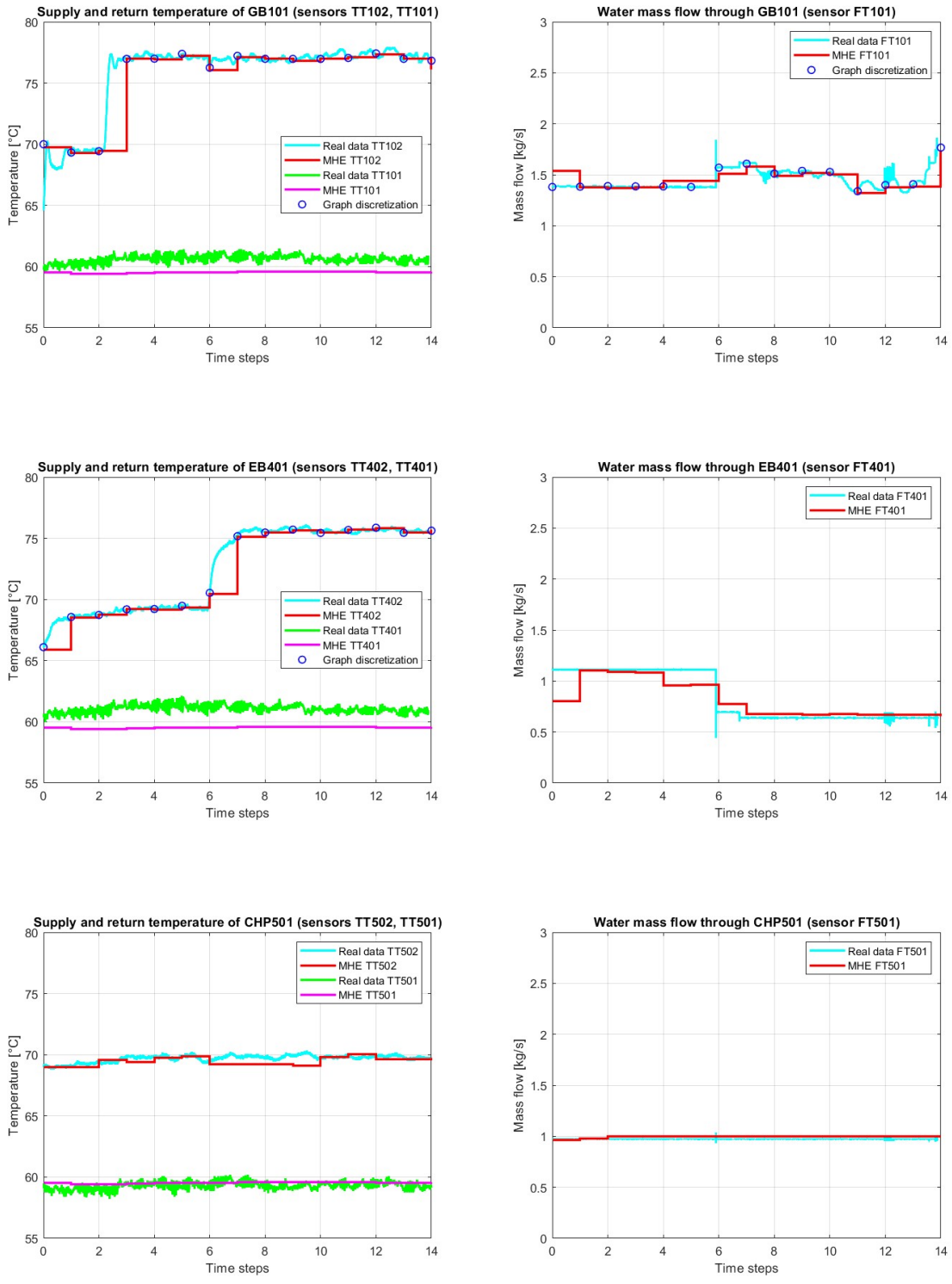

Figure 3.3: Estimations compared with real data: gas boiler sensors TT101 and TT102 (a) and FT101 (b), electric boiler sensors TT401 and TT402 (c) and FT401 (d), CHP sensors TT501 and TT502 (e) and FT501 (f).

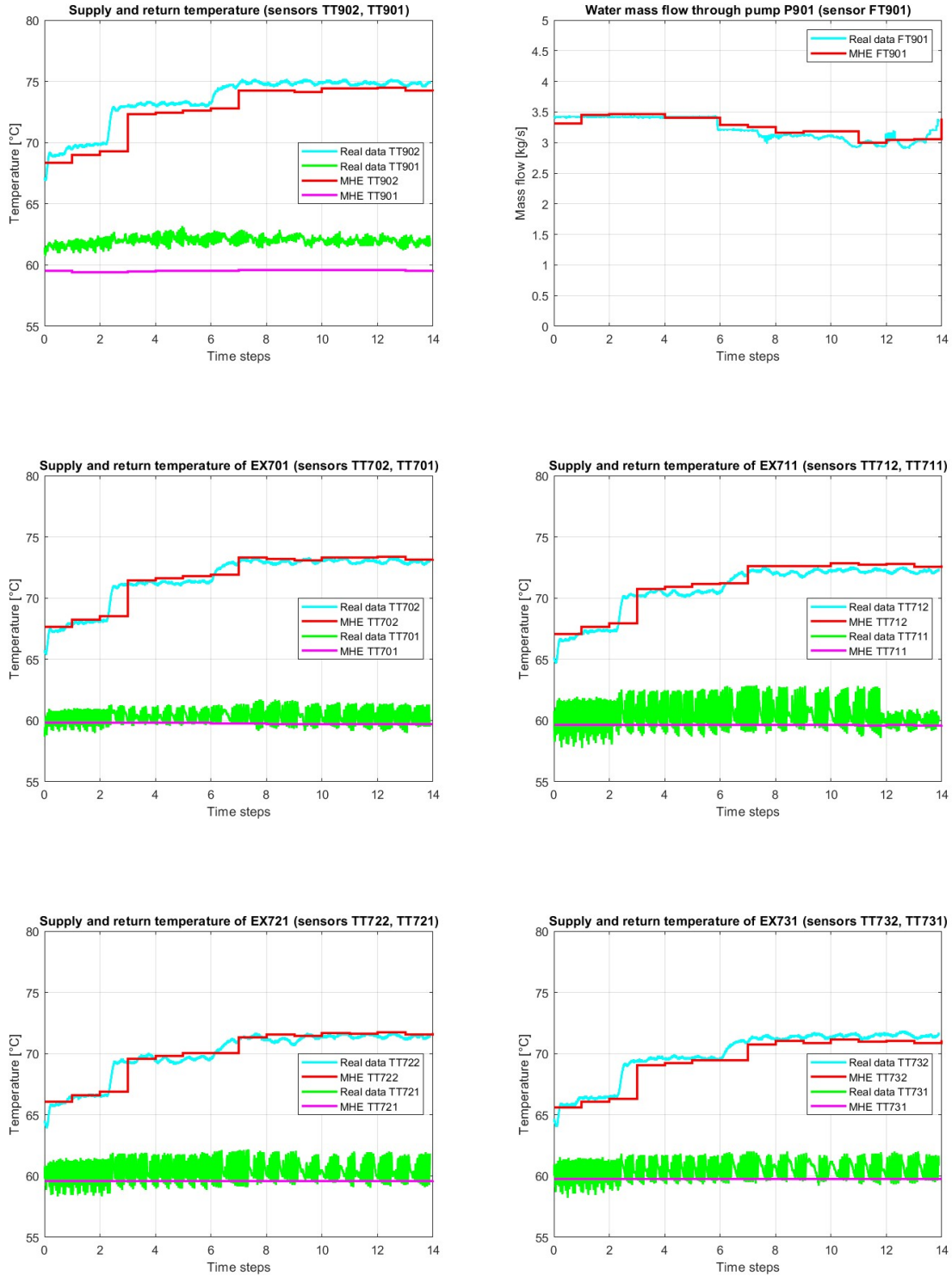

Figure 3.4: Estimations compared with real data: rack distribution sensors TT901 and TT902 (a) and FT901 (b), heat exchangers sensors for supply and return temperatures (c, d, e, f).

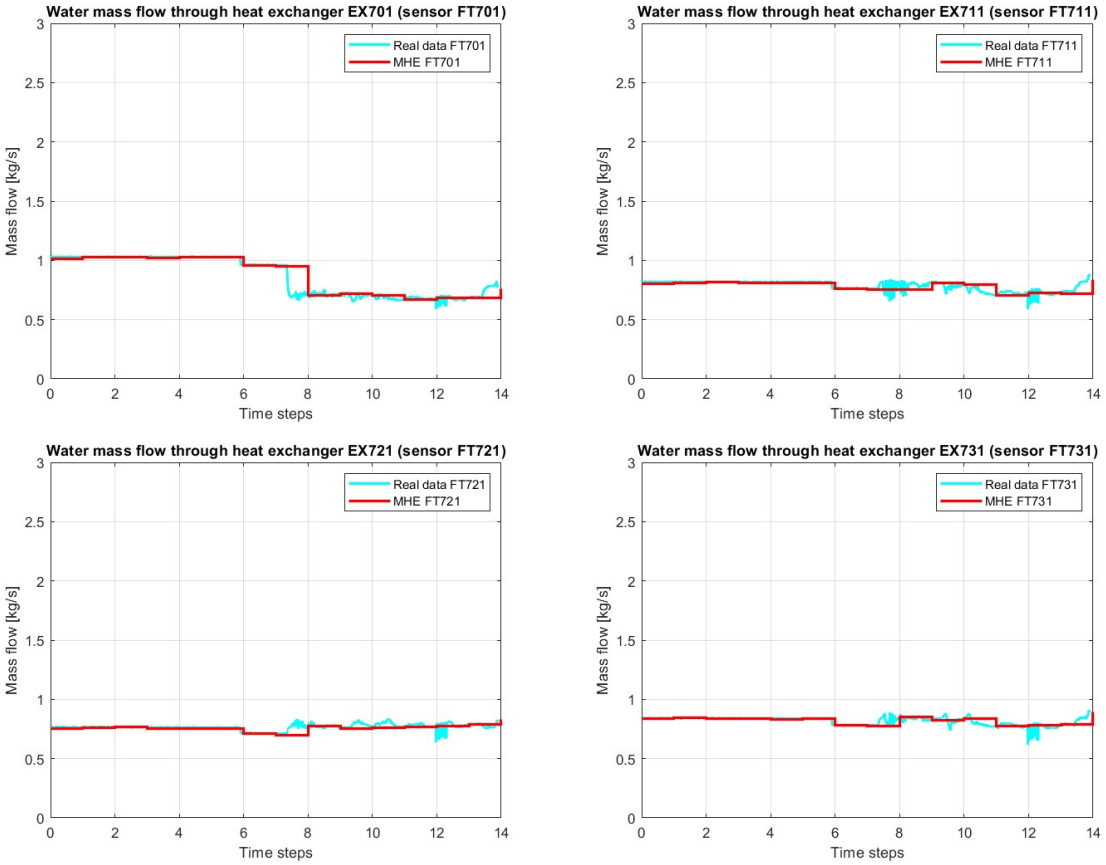

Figure 3.5: Estimations compared with real data: heat exchangers sensors for water mass flow rates.

3.5.1. MHE validation using a different dataset

The Moving Horizon Estimator was further validated using an additional dataset. In this case, a different set of setpoints was applied to the plant, and measurements were collected to verify performance across diverse conditions, ensuring that the estimator was not tailored to just one dataset. This time in fact, a step reference was used only for gas boiler, while keeping electric boiler and CHP' outlet temperatures fixed at 70°C. Idea is again to check that the states profile is correctly met; for conciseness, only a selection of results is presented here, highlighting some of the estimates produced by the MHE. Given that the simulation lasted approximately one and a half hours, a sampling interval of 900 seconds was selected, resulting in a total of 6 time steps.

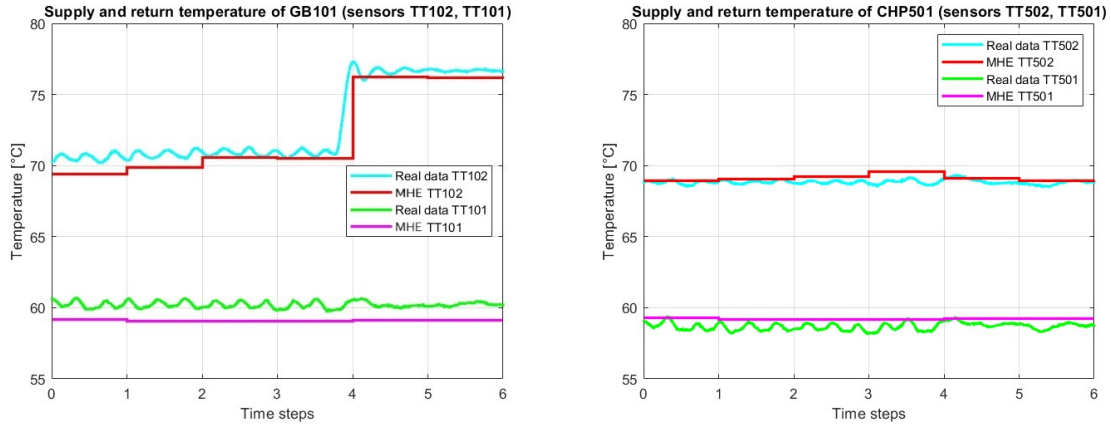

Figure 3.6: Estimations compared with real data: sensors TT101 and TT102 (left), TT501 and TT502 (right).

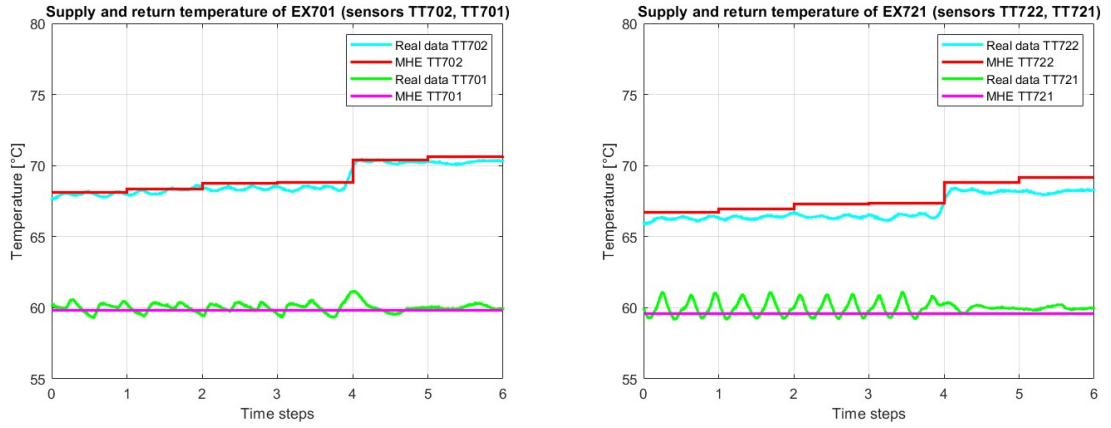

Figure 3.7: Estimations compared with real data: sensors TT701 and TT702 (left), TT721 and TT722 (right).

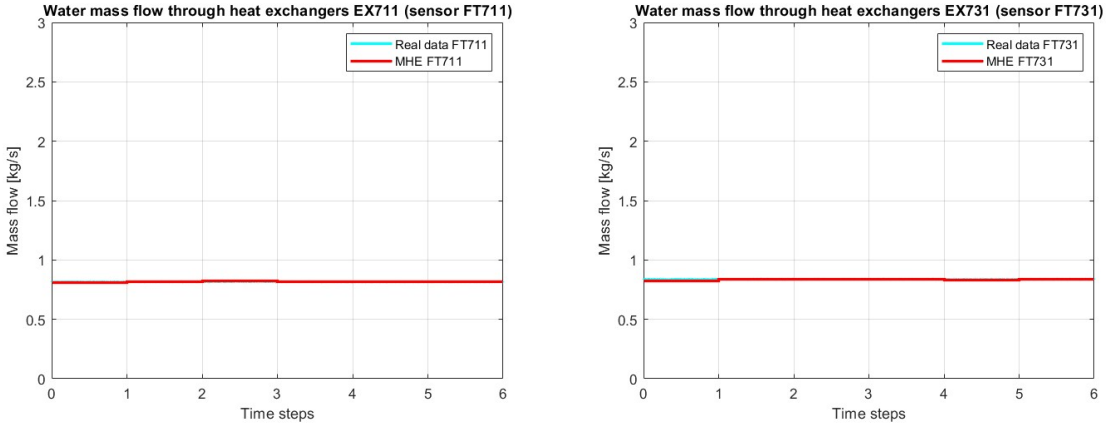

Figure 3.8: Estimations compared with real data: sensors FT711 (left), FT731(right).

3.6. Estimation of unmeasurable states with MHE

To verify that the Moving Horizon Estimator could accurately compute the behavior of all system states, a specific simulation was conducted. In this test, one measurement (TT712: the supply temperature of EX711) was removed from the MHE input matrix "measures." A similar simulation to that described in Section 3.5 was then run. This approach aimed to assess whether the estimator could accurately predict the behavior of an unmeasured system state, demonstrating its capability to estimate states without direct measurements. The outcome, shown in Figure 3.9, demonstrates that an unmeasurable state is effectively matched.

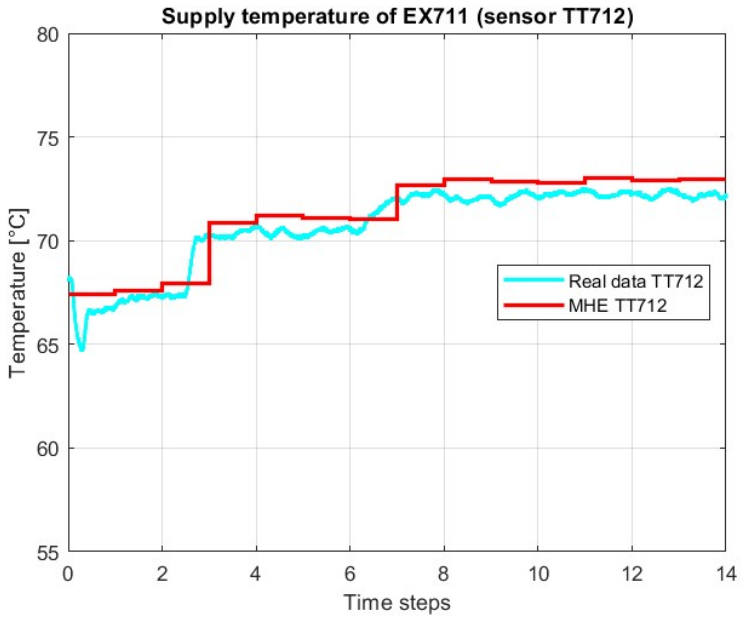

Figure 3.9: Estimation of a system state without providing the measurement to MHE: supply temperature of EX711.

3.7. MHE robustness

Finally, this section highlights a particular feature of the Moving Horizon Estimator, illustrated in Figure 3.10, which shows the water flow rate through the by-pass valve. It can be seen that, although m_{by} measured remains constant at 0.05 $\frac{kg}{s}$, the estimate does not perfectly match the measurement. This is due to MHE's capability to infer system states based on available measurements, while still considering system dynamics.

This characteristic is a significant strength of the estimator, as it enables consistent state estimation even when input data may be inaccurate.

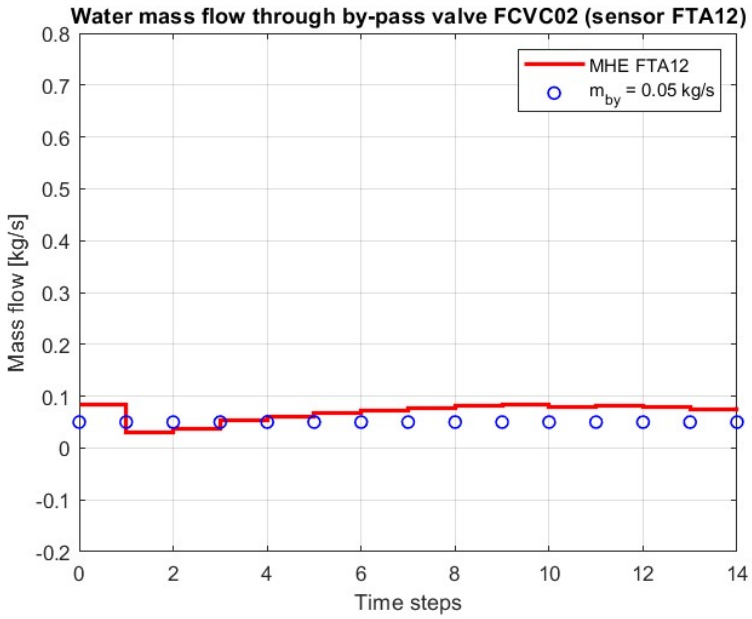

Figure 3.10: Estimation compared with measurement: water flow rate through by-pass valve.

4 | Implementation on the real plant and experimental and results

As already mentioned, the main peculiarity of this thesis is the possibility of testing the designed MPC control scheme, along with the Moving Horizon Estimator, on a real plant, which is the RSE Test Facility. In this chapter the results of all tests performed on the Facility are illustrated and explained.

4.1. Connection MPC - Test Facility

First of all, in this section, it is described how the MPC is able to interface with the real plant. In fact it was necessary to interconnect the Matlab code for MPC and MHE with the Test Facility in order to catch the measurements from sensors and to set the computed control actions to the actuators. This process is managed by the PLC in conjunction with a Python script, while Matlab timers synchronize the various tasks for the estimator and the control scheme. For clarity, a schematization of the exchange of information throughout the system is illustrated in Figure 4.1.

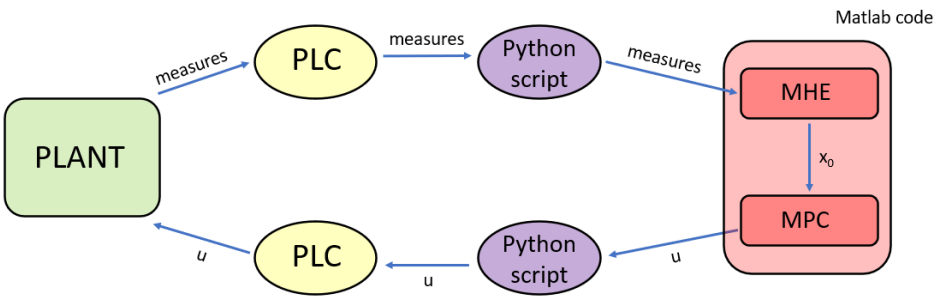

Figure 4.1: General scheme representing the flow of information among the systems involved. The computed control action to be applied is represented by "u", whereas "x_0" stands for the initialization of the MPC.

4.2. Running MHE online

Before running the complete control scheme connected to the Test Facility, only the Moving Horizon Estimator was operated online to verify that information flowed correctly throughout the system. The plant was prepared with a steady-state temperature of 77°C for gas boiler and 68°C for the electric boiler; CHP was kept off due to temporary issues. Loads absorbed power control and return temperature controls were activated to maintain values to 25 kW and 60°C, respectively. Measurements from sensors were read every 10 seconds by the Python and Matlab scripts, with the MHE running simultaneously for a total duration of around 5 minutes. The chosen estimation horizon for MHE was $N = 4$, so that at every iteration only the last four measurements of each sensor were considered. As shown in Figure 4.2, the observer's estimations are sufficiently accurate and also allow to smooth out the return temperature oscillations caused by the PID control. When MHE will be effectively used in conjunction with MPC, Section 4.3, the sampling time will be increased to 15 minutes, and measurements will be passed to the script as the mean of the past data to avoid too large oscillations.

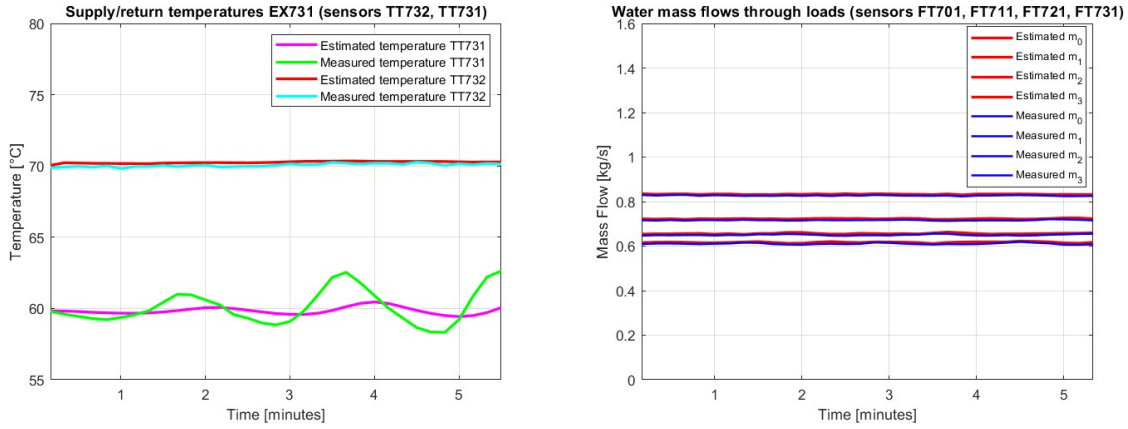

Figure 4.2: Examples of some estimated states using MHE online with 10 seconds of sampling time.

4.3. Real tests on the plant

In this section, the experiments on the real plant are explained and analyzed. As introduced in Section 2.9 for tests in simulation, MPC state and input constraints were set to their physical values, such as maximum and minimum limitations for water temperature and mass flow rate.

CHP outlet temperature was set to a maximum of 70°C, this was done to avoid some

physical issues of the RSE Combined Heat and Power unit which otherwise would shut off.

4.3.1. First test using gas boiler, electric boiler and CHP

This first experiment concerns a Test Facility configuration where all of the three generators were used to produce power. The DHN generators' outlet temperatures were initialized with 80°C for the gas boiler, 75°C for the electric boiler and 70°C for the CHP for the reasons explained in the above paragraph. The resulting mixing water temperature guaranteed an initial steady state for the network of about 72°C in the rack distribution; minimum inlet water temperatures of loads were settled to 72°C in order to have a threshold to not overcome for water temperature arriving at heat exchangers.
Due to the limited time for tests, the absorbed power profile for loads, Figure 1.19, was adapted to last about forty minutes, ranging from 25 kW to 40 KW and maintaining an abrupt pick at the beginning and then slowly decreasing. It can be seen in Figure 4.3. Costs for energy sources were adapted too, using a similar profile to that depicted in Figure 2.18, with the cost of gas constant at 0.60 $/kWh and that of electricity ranging from 0.20 $/kWh to 0.60 $/kWh, as shown in Figure 4.3.

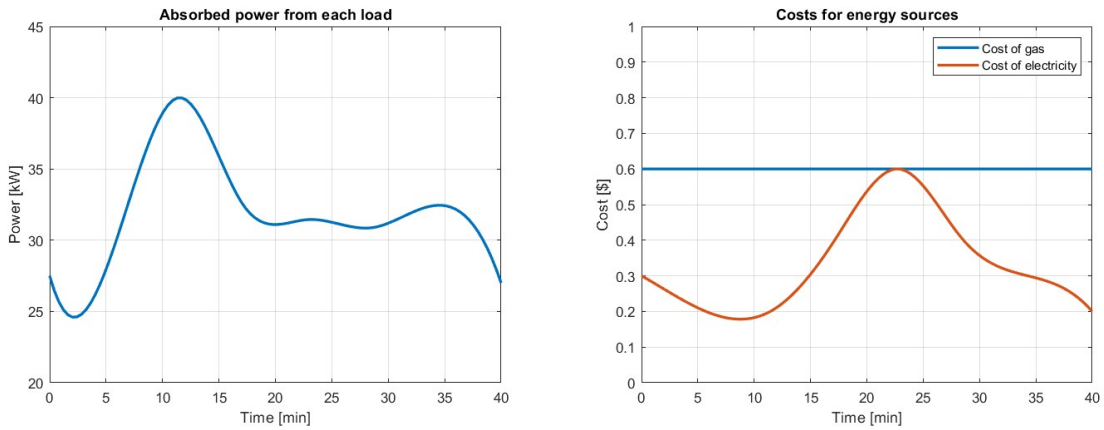

Figure 4.3: Absorbed power setpoint for loads (a) and cost for energy sources (b).

The Model Predictive Control (MPC) was set with a sampling time of 300 seconds, i.e. five minutes, and a prediction horizon of $N = 8$, representing the total number of time steps considered for predictions. The Moving Horizon Estimator used the same sampling interval as the MPC, with a 300-second interval, to compute initialization values for the MPC at each time step. However, the MHE used a shorter horizon window with only four

time steps, leveraging the last four measurements to estimate the system states. At each iteration, the MHE received a new input measurement for each system state. This new input was derived from sensor data collected during the minute prior to MHE activation. Specifically, the mean of the 60 measurements taken (one per second) during the last minute was calculated, and this mean value represented the most recent state data input to the estimator.

For this test, it was decided to keep the water mass flow through electric boiler fixed to the value of 0.75 $\frac{kg}{s}$, the one through CHP in the neighborhood of 0.5 $\frac{kg}{s}$ and the one through gas boiler free to vary. The test was conducted for about forty minutes, expecting the MPC to use the electric boiler at its maximum power, being electricity cost smaller than gas cost, while gas boiler and CHP utilization would be decided based on the most convenient economical situation. Results are expressed here below.

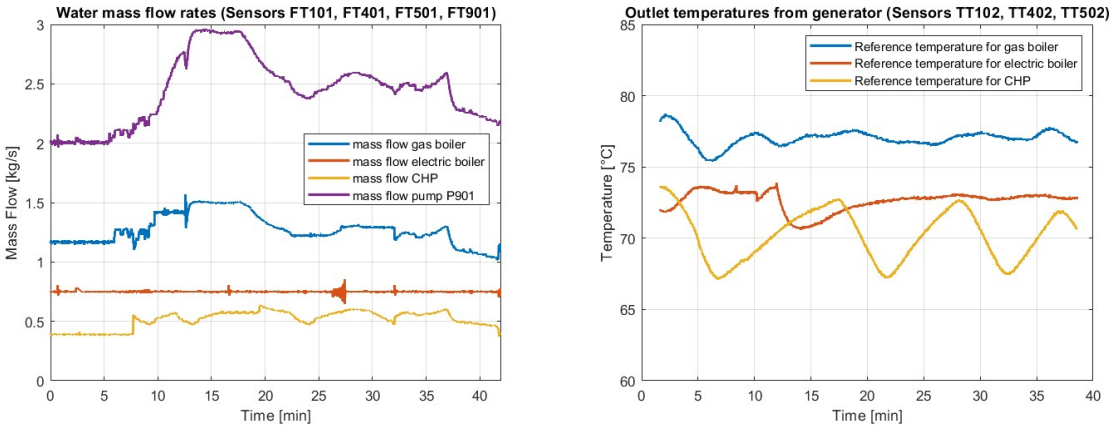

Figure 4.4: Mass flow setpoints for generators and pump P901 (a) and outlet temperatures from generators (b).

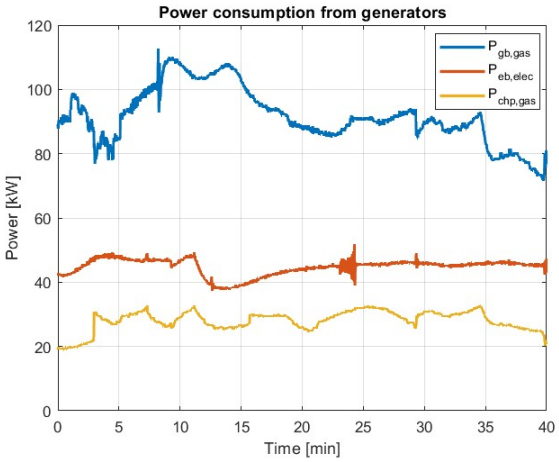

Figure 4.5: Power consumption of the three generators.

Here it's described the way how the Model Predictive Control computed the optimal control actions. As expected, the electric boiler power production was maximized, see Figure 4.5, being the cost of electricity always smaller than that of gas, see Figure 4.3. Since one of the constraints was to keep a minimum value for the inlet water temperature of heat exchangers and knowing that the maximum outlet temperature of CHP could stay only around 70°C, the MPC decision was to maximize the outlet water temperature for electric boiler. Since its mass flow rate was fixed to the value of 0.75 $\frac{kg}{s}$ and giving that the power would be maximized, the reference water temperature of electric boiler was computed in according to the model expressed by Equation (2.6). Coming to the other two generators, the control actions referred to CHP were almost obliged, keeping the water mass flow around the value of 0.5 $\frac{kg}{s}$ and its temperature to the maximum value possible, i.e. 70°C. The oscillating trend of the temperature is due to the physical behavior of the RSE Combined Heat and Power unit. Lastly, the MPC had to decide the way to control the gas boiler. Its reference temperature was set to its maximum possible value of 80°C (to compensate the low value of CHP temperature) and the water mass flow computed consequently, following the model in Equation (2.5). To satisfy the power consumption from users the solution was then to vary the gas boiler water mass flow, increasing it when the absorbed power increased and decreasing it vice versa, as can be seen in Figure 4.4.
For completeness, here are reported also the water temperature arriving at each one of the four exchangers as well as the water mass flow rates, Figure 4.7. It can be seen that the water temperature is constantly around the value of 72°C, while the water flow varies to ensure that the absorbed power matches the profile illustrated in Figure 4.3; its trend correctly follows the one of pump P901 expressed in Figure 4.4, since the quantity of water arriving at each load is a quarter of that passing through the primary pump. Oscillations are due to the power control showed in Section 1.1.5. In Figure 4.7 it's also reported the trend of power effectively absorbed by loads during the whole duration of the experiment; it can be seen that the profile is similar to the reference one, in Figure 4.3.
Finally, this DHN configuration was simulated also on Matlab but with a different control strategy, keeping generators power consumption as constant as possible, in order to observe the actual cost saving brought by the MPC algorithm. Results are expressed in Figure 4.7, where it can be seen that the MPC cost function profile is lower with respect to the one generated by the other control strategy. As done in Section 2.9, the percentage cost saving was computed and the value was 4.27 %; obviously this value is lower with respect to the case where also thermal storage is considered since TES allows for greater efficiency due to the possibility of pre-heat and store water in periods of low costs.

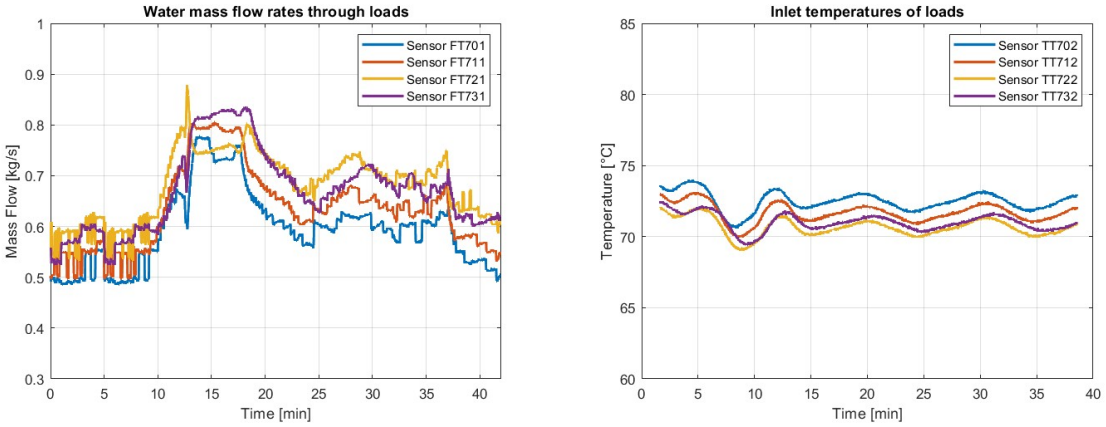

Figure 4.6: Water mass flows through heat exchangers (a) and related inlet water temperature (b).

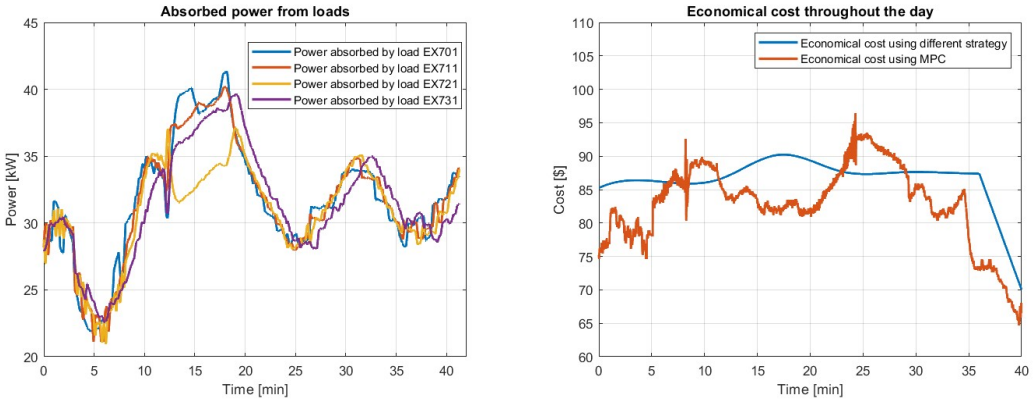

Figure 4.7: Effective absorbed power from loads (a), cost comparison between two control strategies of the same DHN (b).

4.3.2. Second test using gas boiler and electric boiler

The second experiment on the Test Facility was conducted using only gas boiler and electric boiler as generators, reducing the range of operability of the network to 55°C for water in the return pipelines and 60°C/80°C for the supply pipelines. Differently from the previous test, the sampling time for MPC and MHE was set to 900 seconds, i.e. fifteen minutes, making the experiment last two hours. In this test the state constraint referred to the water mass flow through electric boiler was changed, varying between 0.4 $\frac{kg}{s}$ and 0.75 $\frac{kg}{s}$. It was decided to ensure a supply water temperature for loads of at least 62°C. This change aims to observe how the MPC would adjust its control actions. The power absorbed by the heat exchangers is illustrated in Figure 4.8, along with the gas and electricity costs, which in this case have been "inverted" compared to Section 4.3.1: now, the cost of electricity constantly exceeds that of gas. As a result, the Model Predictive

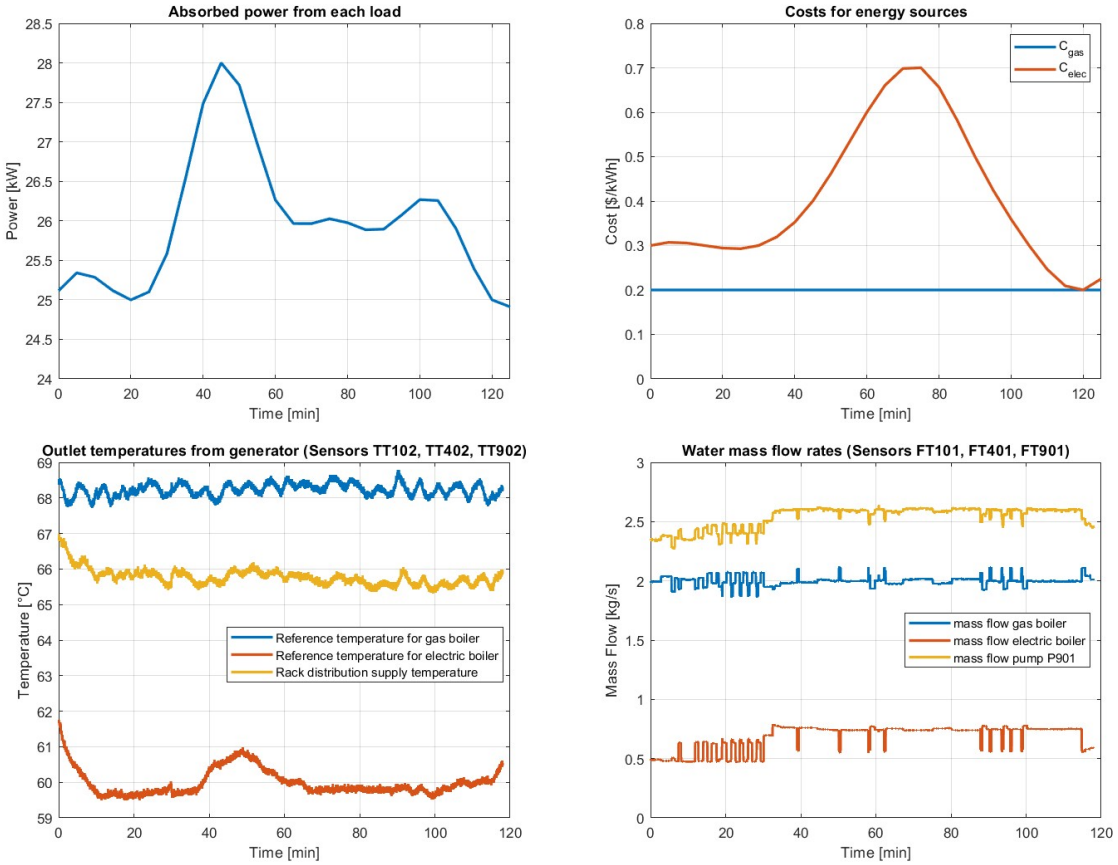

Figure 4.8: Absorbed power from each load (a), costs of gas and electricity (b), reference outlet water temperatures from generators (c), water mass flow passing through generators (d).

Control is expected to prioritize the gas boiler, operating it at maximum capacity, while using the electric boiler only to meet the remaining demand.
As expected, the control actions decided by the Model Predictive Control aimed at using gas boiler at its maximum power, as shown in Figure 4.9, in fact mass flow rate is constantly set at its maximum value (2 $\frac{kg}{s}$) and reference temperature is almost 69°C. On the other hand, the electric boiler is used to meet the remaining loads requests, due to its higher utilization cost. For this reason it can be seen that mass flow rate and reference temperature varies along the duration of the experiment, in particular with the latter picking after forty minutes in correspondence of the moment of high demand. Furthermore, it can be observed that the water mass flow rate is incremented after half an hour until the end; the reason is to ensure the greater power requested (26/28 kW).
Coming to users side, in Figure 4.10 are reported the two quantities characterizing heat exchangers. On the left it's shown the water temperature arriving to loads through the supply pipelines, while on the right the correspondent mass flow rate. It can be seen

that the minimum supply water temperature value, i.e. 62°C, is respected for all loads; temperatures are different due to heat dissipation towards ambient.

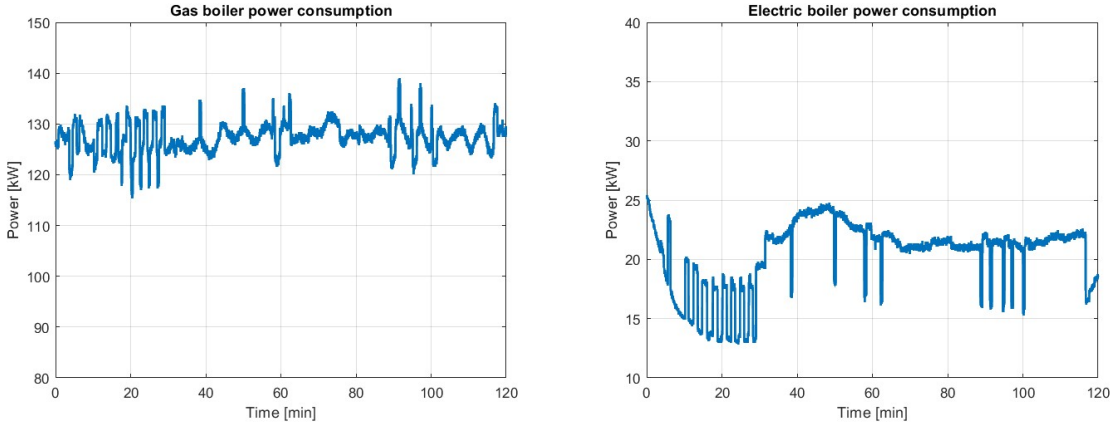

Figure 4.9: Gas boiler power consumption (a), electric boiler power consumption (b).

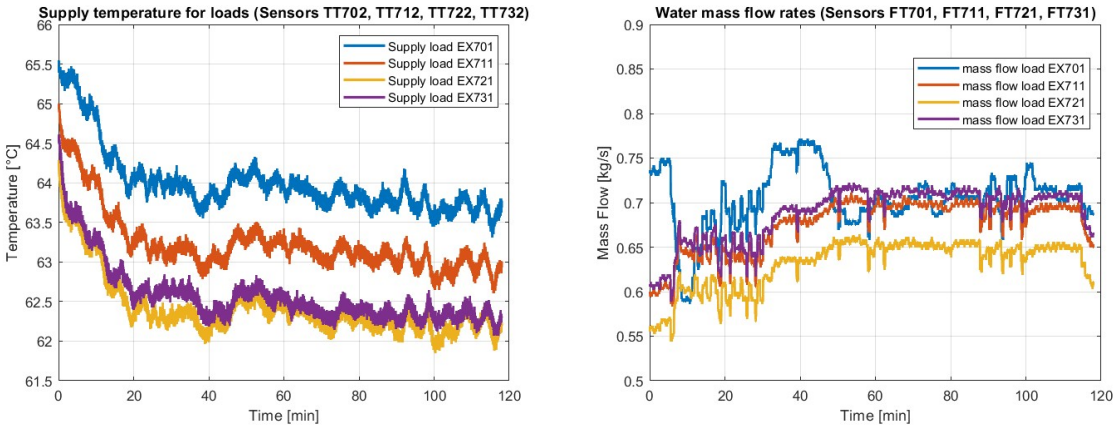

Figure 4.10: Supply water temperature for loads (a), water mass flows through loads (b).

Later on another experiment was carried out, with exactly the same configuration of the above experiment, but controlling the network with almost constant powers from generators and reference outlet water temperatures (satisfying the load demand in Figure 4.8). The idea was to compare the MPC regulation with this control strategy in terms of economical costs. Results, shown in Figure 4.11, demonstrate that an MPC regulation is effectively capable of decrease costs since the computed control actions are the best possible to minimize the cost function. This time, the percentage cost saving is 1.63 %, which is lower compared to the cases in Sections 2.9 and 4.3.1. However, this result was expected since neither the TES nor the CHP was considered in this experiment. In fact, also the Combined Heat and Power unit contributes to significant cost savings by enabling the sale of produced electricity.

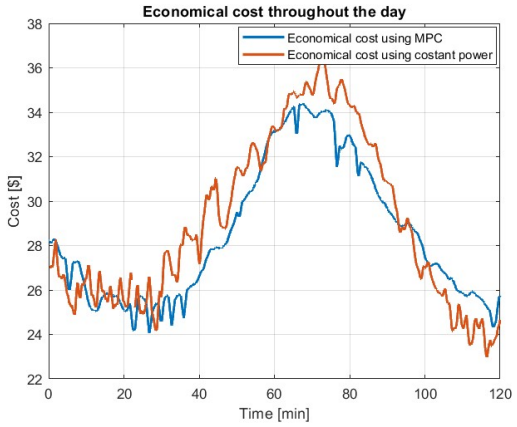

Figure 4.11: Cost comparison between two control strategies of the same DHN.

4.3.3. Similar test changing the minimum supply temperature

This final test is similar to that in Section 4.3.2, but modifying the minimum supply water temperature for loads to the value of 65°C. The absorbed power profile and costs for energy sources remained the same depicted in Figure 4.8 as well as the other state constraints which were not varied. In this case the control actions computed by the MPC are expected to be different from the previous ones, with an increased reference temperature for boilers and consequently a reduced mass flow rate through them. Due to limited time, the experiment did not last two hours as the previous one, but only one hour and a half; anyway, it's meaningful for observing the different decisions of the MPC during the first ninety minutes. Figure 4.12 pictures the computed control actions, i.e. reference outlet water temperatures and their relative water mass flow rates.
As before, in Figure 4.13 there are also reported the graphs of water supply temperatures arriving to loads, which respect the constraint of being above the threshold of 65°C. During the very first iteration, i.e. during the first fifteen minutes, this threshold is not properly respected due to the start up of the MPC.

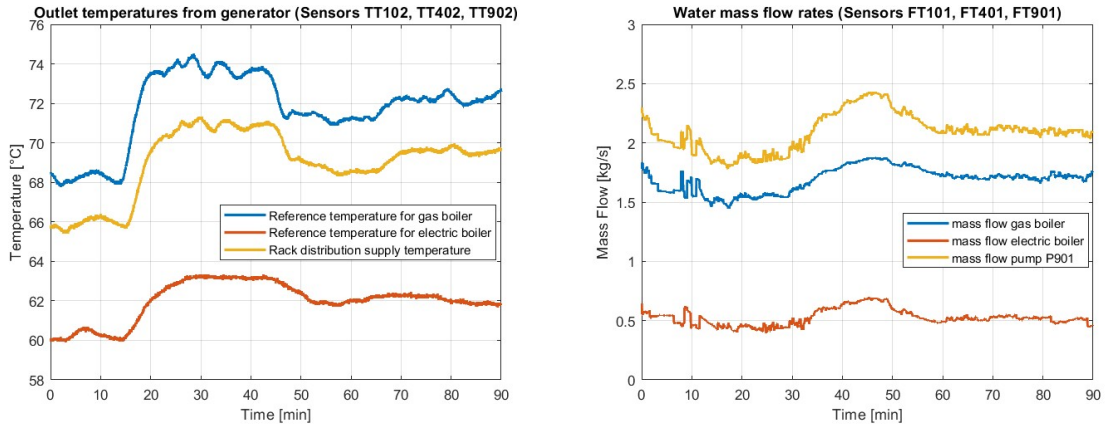

Figure 4.12: Reference outlet water temperatures from generators (a), water mass flow passing through generators (b).

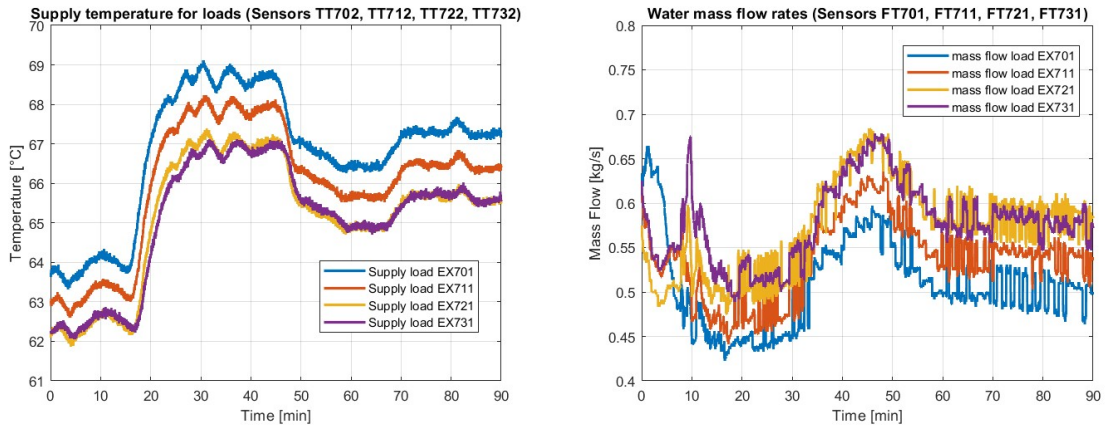

Figure 4.13: Supply water temperature for loads (a), water mass flows through loads (b).

Conclusions and future developments

In the introduction of this thesis, an overview of multi-energy systems was provided, explaining what MES are, the motivations for their increasing use, and the consequent need for optimal control. The case study was then introduced: the RSE Test Facility, a plant that offered the opportunity to test the designed control scheme on a real system.
In Chapter 1, the configuration of the Test Facility was illustrated, highlighting its components, interconnections, and technical specifications. Each network element was then described in detail, along with the physical equations that define the dynamical model. Finally, the Modelica simulator developed by RSE and validated with the real plant was introduced, enabling the study the system's dynamic model.
In Chapter 2 the general formulation of the Model Predictive Control (MPC) problem was given along with the explanation of the reasons why a reduced model for MPC was needed. After that, the latter was described regarding every part of the system illustrating how it was developed for pipes, tanks, gas boiler and the other components. The reduced model was then validated using the Modelica simulator presented in Chapter 1 to check whether it behaved correctly accordingly to the dynamic model. Finally, some tests were settled up on the real plant in order to verify that the state trends computed by the reduced model matched also with the actual behavior of the Test Facility; some little adjustments were done since power losses towards the environment were higher than those in simulation.
In Chapter 3 the issue of having some unmeasurable states was addressed. The Moving Horizon Estimator (MHE) was presented explaining the technique to compute all of the actual system states based on the available measurements from sensors and relying on the reduced model for MPC, which was used also for the estimator. As done for the Model Predictive Control in Chapter 2, also the MHE was validated using the Modelica simulator and then with real data from the plant. Lastly, some strengths of this estimator were highlighted.
In Chapter 4 it is written how the Matlab script for MPC and MHE was actually connected to the PLC of the Test Facility, in order to catch measurements from sensors and give setpoints signals to the actuators. After that, a test to check if the estimator be-

haved correctly was conducted and finally some experiments were carried out to see how the MPC effectively regulated the real Test Facility plant. Tests showed that the MPC decisions changed based on the configuration of network taken into account, on state constraints, but in general the computed control actions were always the optimal ones which minimized the economical cost function.
Future studies could address three main topics. First, introducing a term in the cost function that penalizes pump energy consumption would allow the Model Predictive Control to consider this factor in minimizing economic costs. Second, further studies on Thermal Energy Storage would be beneficial, as TES is a powerful tool for improving District Heating Network efficiency. This includes developing an even more accurate model for TES and conducting real-world tests with thermal storage to observe its actual performance. Lastly, there is significant potential to expand on the tests conducted in this thesis by incorporating additional components. As stated in the introduction, the RSE Test Facility allows for future development and integration of new energy sources. In my opinion, one of the most promising is solar energy, as it could further enhance thermal storage utilization.

Bibliography

[1] C. Anderis. Nonlinear model predictive control of a thermo-hydraulic plant: design and experiments. Master's thesis, Politecnico di Milano, 7 2022.

[2] C. Anderis, M. A. M. Alvarado, and R. Lazzari. Implementation of an experimental facility for district heating networks flexibility assessment. In *2024 AEIT International Annual Conference (AEIT)*, pages 1–6, 2024. doi: 10.23919/AEIT63317.2024.10736713.

[3] H. Bastida, C. E. Ugalde-Loo, M. Abeysekera, M. Qadrdan, J. Wu, and N. Jenkins. Dynamic modelling and control of thermal energy storage. *Energy Procedia*, 158: 2890–2895, 2018.

[4] F. Casella and A. Leva. Modelling of thermo-hydraulic power generation processes using modelica. *Mathematical and Computer Modelling of Dynamical Systems*, 12 (1):19–33, Feb. 2006.

[5] F. Casella and A. Leva. Modelling of thermo-hydraulic power generation processes using modelica. *Mathematical and Computer Modelling of Dynamical Systems*, 12 (1):19–33, February 2006.

[6] R. Dige. Distributed energy generation: The future of clean energy. `https://www.linkedin.com/pulse/distributed-energy-generation-future-clean-ramchandra-dige-jylff/`, 2024. Accessed: 2024-07-01.

[7] S. S. Farahani, Z. Lukszo, T. Keviczky, B. D. Schutter, and R. M. Murray. Robust model predictive control for an uncertain smart thermal grid. In *Proceedings of the European Control Conference (ECC)*, pages 1195–1200, June 2016.

[8] M. Gharbi, F. Bayer, and C. J. Ebenbauer. Moving horizon schätzverfahren - rwth aachen university. `https://www.ic.rwth-aachen.de/cms/ic/forschung/~qxavg/moving-horizon-schaetzverfahren/?lidx=1`. Accessed: 2024-10-12.

[9] IconaClima. Anidride carbonica e gas serra: il riscaldamento glob-

ale, 2024. URL https://www.iconaclima.it/salute-del-pianeta/anidride-carbonica-gas-serra-riscaldamento-globale/. Accessed: August 15, 2024.

[10] IPIECA. Energy efficiency compendium. https://www.ipieca.org/resources/energy-efficiency-compendium, 2024. Accessed: 2024-07-01.

[11] J. Kang, Z. Shao, X. Chen, and L. T. Biegler. Moving horizon estimation - sciencedirect topics. https://www.sciencedirect.com/topics/computer-science/moving-horizon-estimation. Accessed: 2024-10-12.

[12] R. Krug, V. Mehrmann, and M. Schmidt. Nonlinear optimization of district heating networks. *Optimization and Engineering*, 22(2):783–819, Jun. 2021.

[13] R. Krug, V. Mehrmann, and M. Schmidt. Nonlinear optimization of district heating networks. *Optimization Engineering*, 22(2):783–819, June 2021.

[14] S. Lucia and F. Fiedler. Basics of moving horizon estimation. https://www.do-mpc.com/en/latest/theory_mhe.html, 2023. Accessed: 2024-10-12.

[15] L. Magni and R. Scattolini. *Advanced and multivariable control*. Pitagora, 2014.

[16] MathWorks. Matlab. https://it.mathworks.com/products/matlab.html?requestedDomain=, 2024. Accessed: 2024-07-01.

[17] L. Nigro. Hierarchical predictive control of networked multi-energy systems. Master's thesis, Politecnico di Milano, 7 2021.

[18] L. Nigro, A. L. Bella, F. Casella, and R. Scattolini. Control-oriented modelling, simulation, and predictive control of district heating networks. 2023.

[19] L. Nigro, A. L. Bella, F. Casella, and R. Scattolini. Control-oriented modeling, simulation, and predictive control of district heating networks. *IEEE Transactions on Automation Science and Engineering*, 2024.

[20] OpenModelica. Openmodelica. https://openmodelica.org/, 2024. Accessed: 2024-07-01.

[21] S. V. Raković and W. S. Levine. *Handbook of Model Predictive Control*. Birkhäuser, 2019.

[22] M. Rose, H. Gernandt, J. E. Machado, and J. Schiffer. Model predictive control of district heating grids using stabilizing terminal ingredients. *arXiv preprint*, 2024.

[23] G. Sandou, S. Font, S. Tebbani, A. Hiret, and C. Mondon. Predictive control of a

complex district heating network. In *Proceedings of the 44th IEEE Conference on Decision and Control (CDC)*, pages 7372–7377, December 2005.

[24] C. Sandroni, G. Ferrara, G. A. Guagliardi, M. Verga, A. L. Bella, and L. Nigro. Sistemi multienergetici: sviluppo di modelli, architetture di controllo e impianti sperimentali per la validazione delle reti calore. Technical report, RSE, Ricerca sul Sistema Energetico, Via Raffaele Rubattino, 54, 20134 Milano MI, 2022.

[25] K. Sartor, D. Thomas, and P. Dewallef. A comparative study for simulating heat transport in large district heating network. In *Proceedings of the 28th International Conference on Efficiency, Cost, Optimization, Simulation, and Environmental Impact of Energy Systems*, pages 1–27, 2015.

[26] Q. Tan, J. Ma, B. Yang, W. Zhou, W. Zhang, C. Li, X. Zhu, Q. Hu, W. Liu, and L. Zhang. A comprehensive review on sustainable aviation fuel feedstocks, production pathways, challenges, and policies. *Energy*, 281:128104, 2023. doi: 10.1016/j.energy.2023.128104. URL `https://www.sciencedirect.com/science/article/pii/S0360544223009611`.

[27] M. Taylor, S. Long, O. Marjanovic, and A. Parisio. Model predictive control of smart districts with fifth generation heating and cooling networks. *IEEE Transactions on Energy Conversion*, 36(4):2659–2669, December 2021.

[28] United Nations Environment Programme (UNEP). Facts about the climate emergency, 2024. URL `https://www.unep.org/facts-about-climate-emergency`. Accessed: August 15, 2024.

[29] P. R. VAnoli. Corso di termodinamica dei processi di conversione dell'energia: Analisi energetica ed exergetica degli scambiatori di calore, 2007.

[30] M. Verga and S. Casciano. Definizione dei benefici e dei requisiti di un dimostratore multi energy nella test facility di rse. Technical report, RSE, Ricerca sul Sistema Energetico, Via Raffaele Rubattino, 54, 20134 Milano MI, 12 2020.

[31] M. Verga and S. Casciano. Descrizione nel dettaglio della multi energy test facility. Technical report, RSE, Ricerca sul Sistema Energetico, Via Raffaele Rubattino, 54, 20134 Milano MI, 12 2021.

List of Figures

List of Tables

Ringraziamenti

Desidero innanzitutto ringraziare il Prof. Alessio La Bella per la grande disponibilità e pazienza dimostrate durante tutto il percorso, i suoi preziosi consigli sono stati fondamentali in questi mesi. Un sincero ringraziamento va anche al Prof. Riccardo Scattolini, per la fiducia e l'opportunità di affrontare questo progetto di tesi, consentendomi di andare a lavorare sul campo. Un grande grazie anche a l'Ing. Lorenzo Nigro, per la grande disponibilità e per avermi sempre dato una mano qualora ne avessi bisogno, senza la quale non avrei ottenuto questi risultati.
Non posso non ringraziare poi Claudio Anderis, Simone Polimeni, Marcelo Muro Alvarado, Riccardo Lazzari, e tutti gli altri ragazzi di RSE per avermi accolto con simpatia ed avermi sempre aiutato tutti i giorni, offrendomi la possibilità di confrontarmi con un lavoro di questo tipo.
Rivolgo un grande grazie ai miei genitori e fratelli, per la loro presenza e per il sostegno costante durante questo percorso, nonostante i tanti momenti di debolezza.
Ringrazio di cuore la mia ragazza, Ilaria, che mi ha supportato e sopportato durante tutta l'università, restando sempre al mio fianco, anche nei momenti più difficili.
Ringrazio poi tutti gli amici e amiche, la mia squadra di calcio ed i compagni di università, per esserci sempre stati e senza i quali il percorso non sarebbe stato così leggero.
Infine un grande grazie anche a tutti i miei cugini e parenti e un pensiero speciale anche alla mia nonna, alla quale avrei voluto raccontare di questa esperienza e che sono sicuro sarebbe orgogliosa.